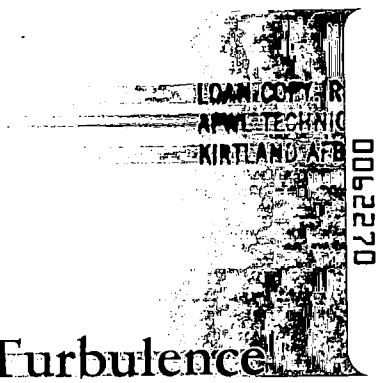

NASA Contractor Report 3378

Case Studies of Clear Air Turbulence Using the Diagnostic Richardson Number Tendency Formulation

John L. Keller and Patrick A. Haines

CONTRACT NAS8-32111
JANUARY 1981

NASA

NASA Contractor Report 3378

Case Studies of Clear Air Turbulence Using the Diagnostic Richardson Number Tendency Formulation

John L. Keller and Patrick A. Haines
University of Dayton
Dayton, Ohio

Prepared for
Marshall Space Flight Center
under Contract NAS8-32111

National Aeronautics
and Space Administration

Scientific and Technical
Information Branch

1981

TABLE OF CONTENTS

LIST OF ILLUSTRATIONS

LIST OF ILLUSTRATIONS (Continued)

LIST OF SYMBOLS

c_p	Specific heat at constant pressure
E	Perturbation energy density
f	Coriolis parameter
H	Height of unstable shear layer
$\vec{i}$	Unit vector (positive = eastward)
I_{CAT}	Index of CAT potential
$\vec{j}$	Unit vector (positive = northward)
P	Pressure
R	Gas constant for dry air
Ri	Richardson number
Ri_{cr}	Critical Richardson number
t	Time
t_{cr}	Time to reach critical Richardson number (Ri_{cr})
u	Eastward component of wind
v	Northward component of wind
$\vec{v}$	Horizontal wind velocity
z	Vertical (height) coordinate
$\lvert\Delta\vec{v}\rvert$	Magnitude of the vertical difference of the horizontal velocity through a given layer
θ	Potential temperature
κ	R/c_p
ρ	Density of air
σ_s	Standard atmospheric static stability
ϕ	Constant related to the Diagnostic Ri tendency
Φ	Diagnostic Ri tendency
χ	Velocity potential
ψ	Stream function
ω	Vertical wind component (DP/Dt)
ω_n	Iterated value of the vertical wind component
ω_N	Final value of the vertical wind component
ω_{qg}	Quasi-geostrophic value of the vertical wind component

FOREWORD

Merely interjecting the word "turbulence" into a conversation with anyone in aviation will elicit an unanticipatable response that depends on the person's experience, education, and role within the aviation community. So many preconceptions and misconceptions are associated with clear air turbulence or "CAT" that it has entered the realm of weather folklore. This research effort was initiated in order to apply recent advances in theoretical research into the CAT mechanism for ultimate operational uses. The initial motivation was, of course, passenger comfort and safety. As is true of many contemporary endeavors, the economics of petroleum changed the perspective. Conversations with some commercial pilots have revealed that flying in turbulent conditions increases fuel consumption "significantly." A decade ago, a change of several percent in aggregate fuel consumption due to essentially random encounters with CAT may not have been significant. Now, the effort needed to detect and forecast CAT and favorably change fuel consumption by just one percent is almost certainly cost-effective. We hope that this report will support the contention that CAT detection and forecasting can be made practical.

This research was conducted by the University of Dayton Research Institute under the auspices of the National Aeronautics and Space Administration, George C. Marshall Space Flight Center, under the technical direction of Mr. Dennis W. Camp of the Space Sciences Laboratory. The support for this effort was provided by Mr. A. Richard Tobiason of Transport Aircraft, Aeronautical Systems Division, Office of Aeronautics and Space Technology.

The authors wish to thank Mr. M. J. Oard, currently of the National Weather Service, for his personal notes and prototype computer source code, and Mr. M. J. O. Dutton of the British Meteorological Office for the detailed records of pilot encounters with CAT. We also wish to thank Mr. Dennis W. Camp for his valuable comments and suggestions about the report manuscript.

INTRODUCTION

Encounters with atmospheric turbulence are an important and persistent problem for the aviation community. Though progress has been made in the communication of turbulence reports to pilots, both commercial and general aviation would benefit considerably by improved forecasting and monitoring of significant regions of moderate to severe turbulence.

When addressing any problem of atmospheric turbulence, it is necessary to distinguish between the two fundamental types of turbulence. The type of turbulence which occurs in the planetary boundary layer (generally in the lower kilometer of the atmosphere) is most important for smaller aircraft but can be significant during takeoffs and landings by high-performance aircraft. This more intense turbulence is generally associated with nonhydrostatic cumulus convection, the most severe being created by thunderstorms. The dangers posed by such storms are due to both the extreme updrafts and downdrafts within the cloud itself and to the outflows at its base. The former problem is generally encountered during in-flight periods, while the latter can present a particularly serious threat during landings. Although strong thunderstorms can often reach to the high levels of flight paths used by high-performance aircraft, their turbulent nature still fits within the framework of nonhydrostatic planetary boundary layer turbulence in which the individual cells can be regarded as a local intrusion of the boundary layer through the free atmosphere.

A most troublesome type of turbulence is associated with statically stable shear layers. While turbulence generated by thunderstorms can usually be avoided by steering clear of the cloud area, turbulence embedded within statically stable shear

layers can often be cloud-free, giving rise to clear air turbulence (CAT). Aircraft observations of CAT indicate that the mean horizontal extent of turbulence is on the order of 100 km in width and approximately 200 km in the direction of the wind. The vertical depth of a layer can be as much as 1500 m. Nearly 50 percent of the time, a patch of CAT can be expected to exist for more than six hours (Pinus, 1964). The commercial and military aviation communities would especially benefit from accurate quantitative monitoring and prediction of CAT. This is due to the fact that commercial airlines tend to fly near the tropopause level where statically stable shear layers are more common.

What is the motivation for developing and implementing improved turbulence detection and forecasting techniques? The reason which initially formed the basis for earlier work remains: passenger comfort and safety. However, a more contemporary motivation has been added. Pilots report that fuel consumption rates increase perceptibly while flying in turbulent conditions (Camp and Frost, 1980). Avoiding turbulence can save money.

With the development of the FPS-16 Jimpshere/Jimsonde (J/J) balloon system came the capability for obtaining high resolution profiles of wind, temperature, and rise-rate (e.g., Fichtl, 1971; Camp and Caplan, 1969; Range Commander's Council Document, 110-77, 1977). The resolution appears sufficient to accurately sense the vertical structure of mesoscale disturbances which support the CAT producing mechanism, i.e., unstable Kelvin-Helmholtz gravity waves created within statically stable shear layers (e.g., Lalas, et al., 1976; Lalas and Einaude, 1976; Lindzen and Rosenthal, 1976). Unfortunately, the existence and intensity of the turbulence can only be inferred from statistical considerations of a given stratified shear layer, under an assumption of Kelvin-Helmholtz (K-H) instabilities, as resolved by a J/J profile (e.g., Essenwanger and Reiter, 1969;

Keller, 1978). The expense of implementing an operational J/J system does not appear to be justified by its potential usefulness as a CAT detector.

Currently, operational turbulence forecast products supplied to the aviation community are generally considered to be highly imprecise and often inaccurate. In effect, the synoptic scale information obtained by the Rawinsonde (RW) observations acts merely to supplement airline pilot reports of turbulence encounters. There would appear to be more practical merit in using the existing operational RW more effectively. Such an approach, the Diagnostic Richardson number Tendency (DRT) technique, involves the calculation of vertical wind shear, static stability (and hence the Richardson number), and their tendencies at the synoptic scale.

The Richardson number is defined as

$$Ri = \frac{-1}{\rho} \frac{\partial \ln\theta}{\partial P} \Big/ \left| \frac{\partial \vec{v}}{\partial P} \right|^2 , \qquad (1)$$

with

ρ = density,
θ = potential temperature,
P = atmosphere, and
$\vec{v}$ = horizontal wind velocity.

The most recent formulation of the DRT technique is that of Oard (1974). Oard demonstrated the potential usefulness of the DRT technique by applying the technique to a previously well-documented CAT event (Reed and Hardy, 1972). The indices produced by the Oard formulation of the DRT technique corresponded well to regions where documented aircraft encounters had occurred.

In a more recent investigation (Dutton, 1979) indices corresponding to the DRT predictors were evaluated for their correlation to documented moderate to severe CAT encounters experienced during trans-Atlantic flights. Dutton found

these indices correlated poorly to the encountered regions of CAT. However, Oard contended that very accurate values for the vertical wind velocity (ω) were necessary for the calculation of the DRT indices. Thus, Oard used vertical velocities determined from an iteration of the "Balance ω equation" to obtain highly refined diagnostic ω's. The vertical velocities used by Dutton (1979) were a forecast product of the 10-level model currently used by the British Meteorological Office (Burridge and Gadd, 1977). Prognosticated ω's are generally considered to be inaccurate. Thus, since accurate values of ω are required to give reasonable DRT indices, the results of Dutton's study are not too surprising. Dutton also calculated, from the prognostic model output, an index which he found to have forecast skill with respect to CAT. These regions will be compared with the DRT indices in the results of this report.

An index for quantitatively measuring the potential for CAT has been defined (Roach, 1970) using the time rate of change of the Richardson number (Ri) following the air motion. This is the so-called Diagnostic Ri Tendency (DRT). Ignoring small terms, it is

$$\Phi \equiv -\frac{D}{Dt}\,\ell nRi = 2\left|\frac{\partial\vec{v}}{\partial P}\right|^{-1}\frac{D}{Dt}\left|\frac{\partial\vec{v}}{\partial P}\right| - \left(\frac{\partial\theta}{\partial P}\right)^{-1}\frac{D}{Dt}\left(\frac{\partial\theta}{\partial P}\right) \qquad (2)$$

where

$$\frac{D}{Dt} \equiv \frac{\partial}{\partial t} + \vec{v}\cdot\nabla + \omega\frac{\partial}{\partial P} \quad \text{and}$$

$$\omega = \frac{DP}{Dt}\ .$$

The initial application of Eq. (2) in a case study (Roach, 1970) encountered problems which arose primarily due to the method of calculating the first term on the right, the vertical wind shear tendency. This shortcoming was greatly remedied by using the thermal wind to specify the vertical shear tendency (Oard, 1974).

Following the method of Haltiner and Martin (1957), the vertical wind shear tendency is expressed in terms of isotherm packing related to frontogenesis, i.e.,

$$2\left|\frac{\partial\vec{v}}{\partial P}\right|^{-1}\frac{D}{Dt}\left|\frac{\partial\vec{v}}{\partial P}\right| = 2Rf^{-1}p^{\kappa-1}\left|\frac{\partial\vec{v}}{\partial P}\right|^{-1}(1000)^{-\kappa} \qquad (3)$$

$$\times\left[-\frac{\partial\theta}{\partial x}|\nabla\theta|^{-1}\left(\frac{\partial\theta}{\partial x}\frac{\partial u}{\partial x} + \frac{\partial\theta}{\partial y}\frac{\partial v}{\partial x} + \frac{\partial\theta}{\partial P}\frac{\partial\omega}{\partial x}\right) - \frac{\partial\theta}{\partial y}|\nabla\theta|^{-1}\right.$$

$$\left.\times\left(\frac{\partial\theta}{\partial x}\frac{\partial u}{\partial y} + \frac{\partial\theta}{\partial y}\frac{\partial v}{\partial y} + \frac{\partial\theta}{\partial P}\frac{\partial\omega}{\partial y}\right)\right]$$

The second term, the static stability tendency, is expressed as

$$-\left(\frac{\partial\theta}{\partial P}\right)^{-1}\frac{D}{Dt}\left(\frac{\partial\theta}{\partial P}\right) = \left(\frac{\partial\theta}{\partial P}\right)^{-1}\left(\frac{\partial\theta}{\partial x}\frac{\partial u}{\partial P} + \frac{\partial\theta}{\partial y}\frac{\partial v}{\partial P} + \frac{\partial\theta}{\partial P}\frac{\partial\omega}{\partial P}\right) \qquad (4)$$

where

R = gas constant for dry air,
c_p = specific heat at constant pressure,
$\kappa = R/c_p$,
f = coriolis parameter,
u = eastward component of wind,
v = northward component of wind,
ω = vertical component of wind, and
∇ = "del" operator.

The meteorological variables of u, v, and θ can be obtained more-or-less directly from the synoptic data network. Details of the input data procedure will be discussed later. One possible weakness of this formulation, as was pointed out by Oard, is its reliance exclusively on the thermal wind approximation for the vertical wind shear. The vertical velocity, ω, must be obtained indirectly. Since accurate values are required, the field is obtained through an iterative solution of the full balance ω-equation using quasi-geostrophic ω's for the initial guess field.

The primary index for CAT used by Oard (1974), obtained from Eq. (2), is defined as

$$t_{cr} = \ell nRi/(\Phi) \tag{5}$$

which is an idealized measure of the time required by an atmospheric layer to reach the critical value of the Richardson number (Ri_{cr}) assuming the atmosphere continues the trend at the instance of observation. The value of Ri_{cr} for an infinitesimal layer has been found theoretically to be 0.25 (Miles and Howard, 1964). Since such a condition would never be resolved due to the synoptic scale nature of the Rawinsonde network input data, Oard arbitrarily chose $Ri_{cr} = 1$. Given the idealistic nature of t_{cr}, the primary usefulness of t_{cr} as a relative measure of CAT development probability remains intact.

It can readily be seen from Eq. (5) that regions where $\Phi << 0$ and Ri is relatively small are regions which would be prime candidates for supporting CAT (i.e., give small t_{cr}). Such a conclusion is supported by the results of the case study performed by Oard (1974) and by the results of this work, which will be discussed later. While Eq. (5) takes into account vertical shear with respect to the time required for the atmosphere to reach a state favorable for the initiation of turbulence, a given value of t_{cr} will not uniquely imply what its potential intensity will be. Thus, based upon what is now known about the nature of the CAT mechanism, a modification of this index is also considered. Both the index used by Oard and this latter index are calculated and compared to documented CAT encounter reports.

In the many empirical, theoretical, and numerical studies of CAT if any one element were to be considered to play a dominant role for both the initiation of turbulence and determining its intensity, it is the variation of the horizontal wind velocity with height, the vertical wind shear. It has been shown (Roach, 1970; Lindzen, 1974) that the vertical shear plays a dominant role as the energy source for K-H instabilities and that for a hyperbolic tangent shear profile, the rate of increase of K-H perturbation energy is proportional to the cube of the shear amplitude (Lalas and Einaudi, 1976; Haines, 1980), that is

$$\frac{d}{dt}\int_{-H}^{\infty} E\,dz \propto |\Delta\vec{v}|^3 \qquad (6)$$

where

E = perturbation energy density, and
H = height of unstable shear layer.

The energy being fed into the amplifying K-H instabilities ultimately cascades into the turbulent subrange. An additional consideration is based upon the theoretical revelation that the unstable K-H wave is carried along by the larger scale wind

field. Such behavior seems to be substantiated by recent observations (Gary, 1980). Hence, one is confronted with the situation where patches of CAT produced in some source region are propagated away and may be maintained as long as the larger-scale shear is sufficiently large. Figure 1 schematically illustrates the CAT producing mechanism as it is currently believed to operate in the free atmosphere.

From left to right, Figure 1 shows the creation of larger, synoptic-scale statically stable shear layers within which smaller-scale discontinuities can exist. These shallower layers can then absorb gravity wave energy due to cumulus convection, terrain, or other random sources below through critical layer absorption (e.g., Hines, 1968; Bretherton, 1969; Jordan, 1972). Amplifying K-H instabilities may then form at these levels, ultimately "breaking" to form turbulence. That the spectra of breaking K-H instabilities are consistent with the observed turbulent spectra was shown by Reiter (1969). Despite the consistent results shown by Haines (1980) in his K-H wave energetical analyses of detailed J/J profiles, the fact that it is the RW system and not the J/J system which is currently operational compels the development of an index which is valid for the RW resolution.

An index has been devised accounting for the role of vertical shear, as determined from RW observations, with respect to the potentially available energy for K-H instabilities. The rate of turbulent energy dissipation in an unstable shear layer was determined, based upon the synoptic-scale origin of the energy destined to become turbulent motion by Roach (1970), as

$$\bar{\varepsilon} = \begin{cases} \frac{|\Delta\vec{v}|^2}{24}\,\Phi\,, & \Phi > 0 \\ 0\,, & \Phi \leq 0\,. \end{cases} \qquad (7)$$

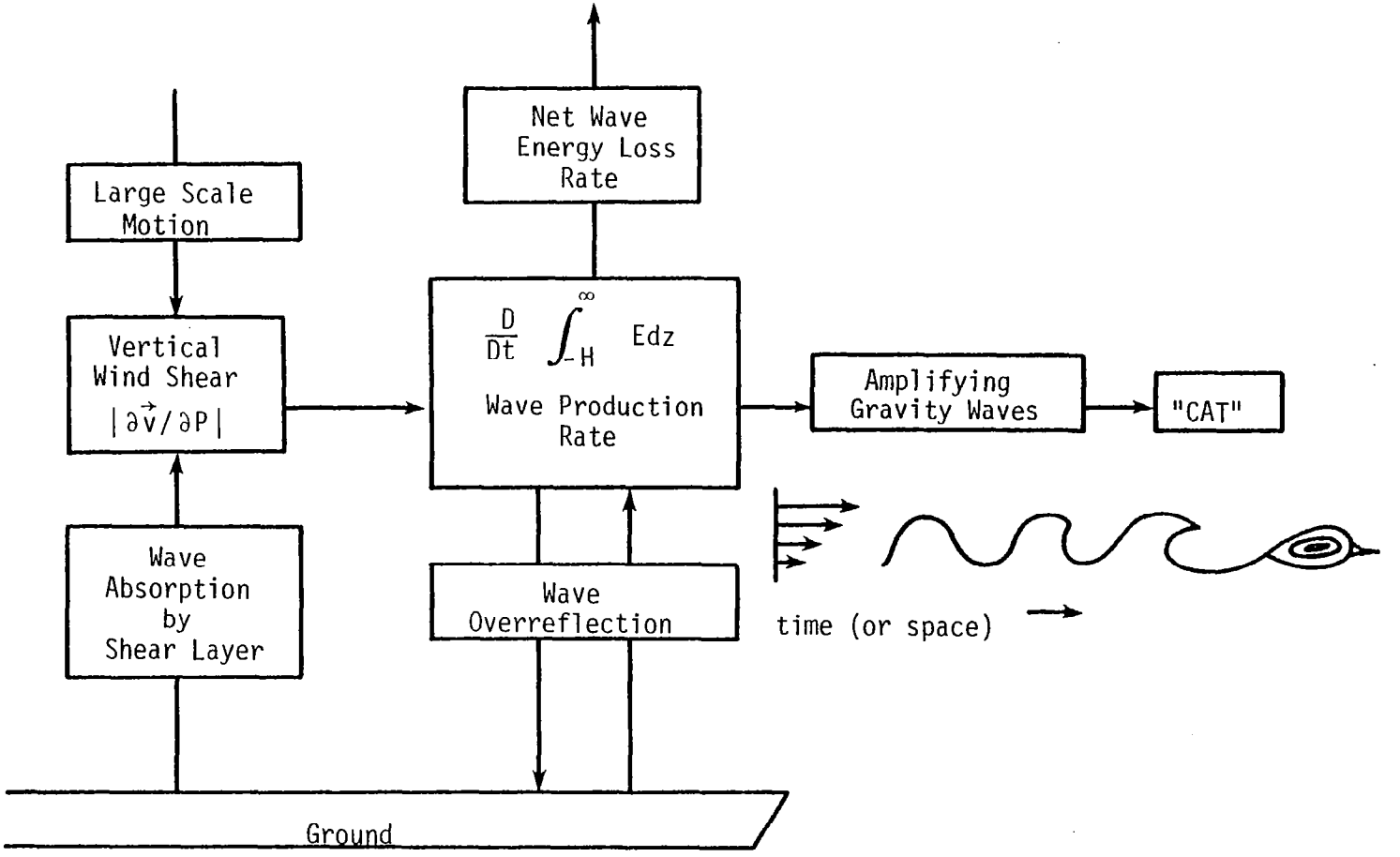

Figure 1. The CAT mechanism.

The value of $\bar{\epsilon}$ has units of energy per unit time. Upon inspection it can be seen that Eqs. (6) and (7) are differing functions of $|\Delta\vec{v}|$. This is because they are actually measures of different quantities. Equation (6), in its complete form, includes factors involving the growth rate of a given unstable K-H wave obtained from a normal-mode instability analysis with respect to a given highly idealized vertical wind profile. Thus, Eq. (6) represents the amplification rate of a single K-H mode. Alternatively, Eq. (7) is essentially a measure of the "rate of accumulation" of the energy potentially available to K-H instabilities within a given synoptic-scale volume of atmosphere. As well, since Eq. (7) takes into account the contribution of the surrounding atmosphere (via Φ), it is a much more physically realistic model than the highly idealized model which is the source of Eq. (6).

In practice a value of $|\Delta\vec{v}|^2$ is calculated by

$$|\Delta\vec{v}|^2 \simeq \left|\frac{\partial\vec{v}}{\partial P}\right|^2 (\Delta P)^2 \tag{8}$$

where

$$\Delta P = 100 \text{ mb.}$$

A modified form of Eq. (7) was used as an index of CAT potential,

$$I_{CAT} = |\Delta\vec{v}|^2(\Phi + \phi) \tag{9}$$

The constant ϕ is included to take into account potentially turbulent situations where Φ is small and oscillating around zero. Thus, I_{CAT} could be large (due to large $|\Delta\vec{v}|$), locally supporting turbulent layers where $Ri \to 1/4$. The value of ϕ is chosen to be $-2.5 \times 10^{-6} s^{-1}$ which is small enough not to affect significantly large positive values of Φ. I_{CAT} is set equal to zero for all $I_{CAT} < 0$. It might just as well have been kept negative and used as an indicator of "low-risk" areas. However, to provide clearer graphical display, the former choice is made.

The turbulent energy dissipation rate, $\bar{\varepsilon}$, defined by Eq. (7) is strictly valid only within the relatively shallow statically-stable shear layer itself where Ri approaches 1/4 and unstable K-H waves can exist. Thus, the use of Eq. (7) would require the same vertically detailed data as does Eq. (6) which is available only via special data systems such as the J/J system. The modified expression Eq. (9) is applied to fixed synoptic-scale vertical increments (ΔP = 100 mb) resolved by the RW system which may contain these shallow layers of unstable K-H waves. The situation of relatively shallow CAT layers existing within synoptic scale layers of the atmosphere was discussed by Roach (1970) who suggested an attempt should be made to statistically relate mesoscale Richardson numbers for which Eq. (7) is valid to synoptic-scale Richardson numbers. This analysis was ultimately performed using conjunctive RW and J/J balloon profiles (Keller, 1978). Unfortunately, neither the Richardson numbers nor the vertical shears proved to be consistently related. Hence, the factor 1/24 in Eq. (7) is dropped and Eq. (9) becomes a relative measure of CAT potential, with an implicit understanding that it should be interpreted in terms of the probability for the existence of one or more CAT layers embedded somewhere within the given synoptic layer. The units remain as energy per unit time, which can be interpreted physically as a rate of generation (or as stated earlier, "rate of accumulation") of the energy potentially available to K-H instabilities.

An assumption whose effects remain as in the Oard study is that of the adiabatic assumption

$$D\ell n\theta/Dt = 0 \qquad (10)$$

used in the derivation of Eq. (4) the static stability tendency. This assumption is valid in the absence of radiation effects and in relatively dry air. Since the main interest is with respect to turbulence in clear air, Eq. (10) would seem to be a reasonable approximation.

GENERAL NATURE OF INPUT DATA

In this case study Oard graphically generated from the raw RW ascent data a grid consisting of 15 × 15 points in the horizontal at 10 constant pressure levels. This corresponded to a horizontal resolution of 250 km and 100 mb vertical resolution. Each data-set required about two to three months of effort to construct. It is not surprising, then, that Oard investigated only one case of CAT.

Such a methodology for generating input data-sets is obviously impractical for case study applications of the DRT approach. In this study, a DRT data preprocessor was developed which uses the archived National Meteorological Center (NMC) formatted data. A 15 × 15 point grid, consisted of a subset of the NMC 1977 point octagonal grid, can be specified for virtually any area of interest in the Northern hemisphere (see Figure 2). This corresponds to a horizontal resolution of approximately 360 km for cases that are considered prior to 1 July 1978. Starting at this date, the horizontal resolution has doubled to approximately 180 km.

The DRT data preprocessor provides to the DRT model, for an arbitrarily specified geographic region, a "data-net" of horizontal wind velocity, $\vec{v}$, pressure height, z, and temperature, T, at 19 constant pressure surfaces from 100 to 1000 mb. This corresponds to vertical resolution of 50 mb--twice that of the input data-sets of Oard. The NMC gridded data, obtained from archived NMC data tapes, exists at the standard pressure levels: 100, 150, 200, 250, 300, 400, 500, 700, and 850 mb. Only $\vec{v}$ and z are available at 1000 mb. This fact requires interpolated data fields to be created at 350, 450, 550, 600, 650, 750, 800, 900, and 950 mb as well as extrapolation for T at 1000 mb. This task is performed by simple linear interpolation (Bevington, 1969).

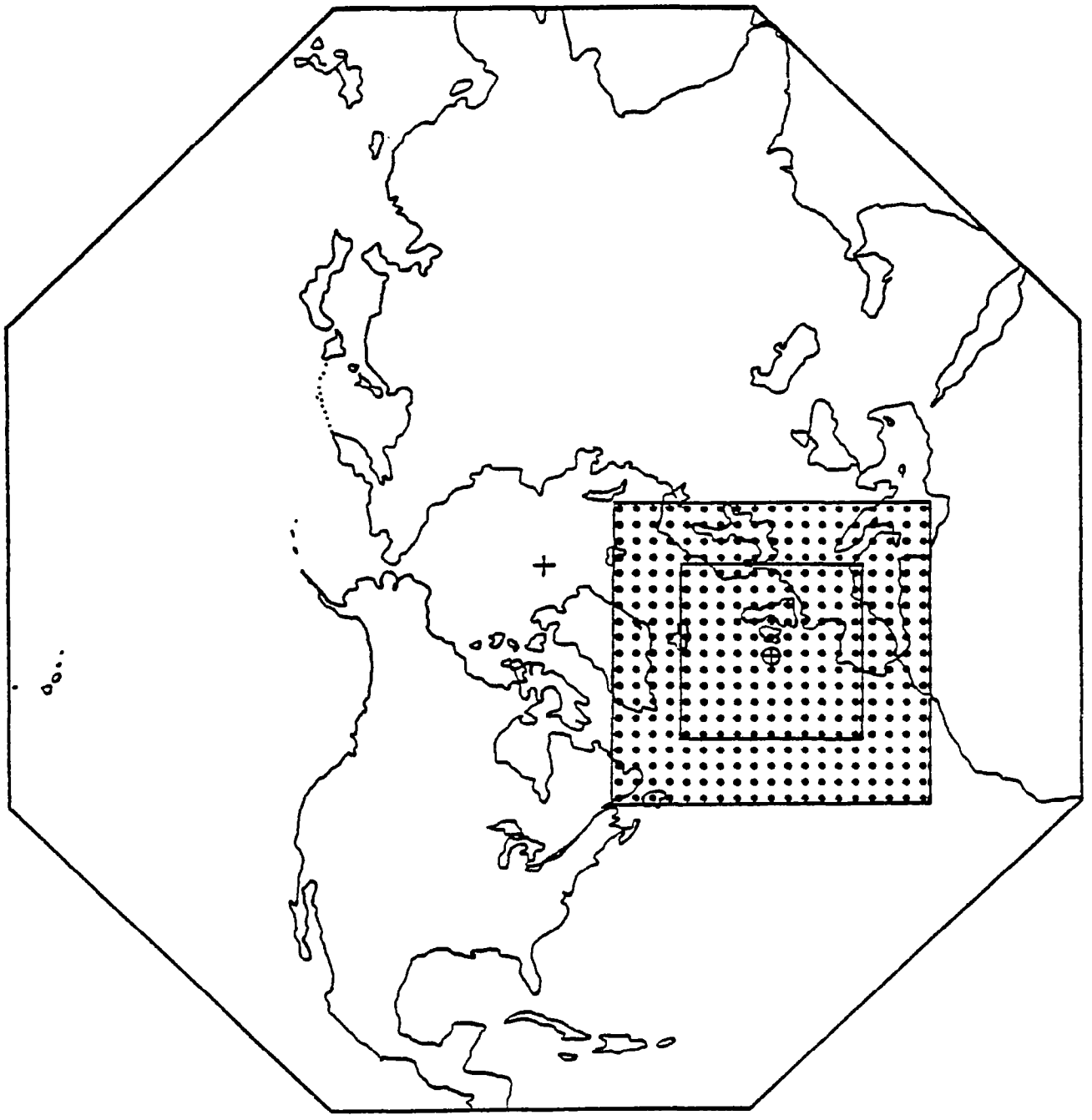

Figure 2. DRT horizontal grid as subset of the NMC octagonal hemispheric grid. The outer square encompasses the input data grid. The inner square encompasses the output grid.

The scalar T and z fields can be interpolated in this fashion with relative impunity. However, strictly speaking, the horizontal wind velocity, $\vec{v}$, should not be handled simply by interpolating its components u and v (e.g., Luers and MacArthur, 1975; Schaefer and Doswell, III, 1979). Accurate interpolation would require the decomposition of $\vec{v}$ into its stream-function and velocity potential which could then be interpolated and finally used to obtain $\vec{v}$ at the necessary levels (Shukla and Saha, 1974). The current version of the DRT data preprocessor uses linearly interpolated values of $\vec{v}$ based upon the contention that the results obtained would be changed only in minor detail. The reasons are as follows: (a) the vertical motion (ω) field can be obtained iteratively, requiring only a rough initial guess field, (b) the region of greatest interest is generally above 350 mb where interpolation of $\vec{v}$ is not required, and (c) a sensitivity analysis was performed (Keller, et al., 1979) which indicates that the important features of areas of high CAT potential are essentially maintained even for significantly disturbed wind fields.

Figure 3 shows the DRT case study methodology. The NMC formatted data fields for the map time corresponding to pilot documented CAT encounters are addressed by a data preprocessor. As detailed earlier, the data preprocessor supplies the required $15 \times 15 \times 19$ "data-net" of $\vec{v}$, z, and T to the DRT module which calculates t_{cr} and I_{CAT}. The DRT module, formulated in Section 2, is outlined in Figure 4. The primary task performed by the DRT module is the calculation of Φ, the Ri tendency. The values of $|\partial\vec{v}/\partial P|$ and Ri, which are factors in the indices t_{cr} and I_{CAT}, are calculated directly from the input data. The Ri tendency, Φ, is a function of $\vec{v}$, T, and ω_N, the balance vertical velocity. The Balance-omega, ω_N, is obtained iteratively using the quasi-geostrophic omega (ω_{qg}) for the initial guess (ω_1).

Consider Figures 5, 6, and 7. Figure 5 compares the magnitude of unperturbed and the randomly perturbed eastward

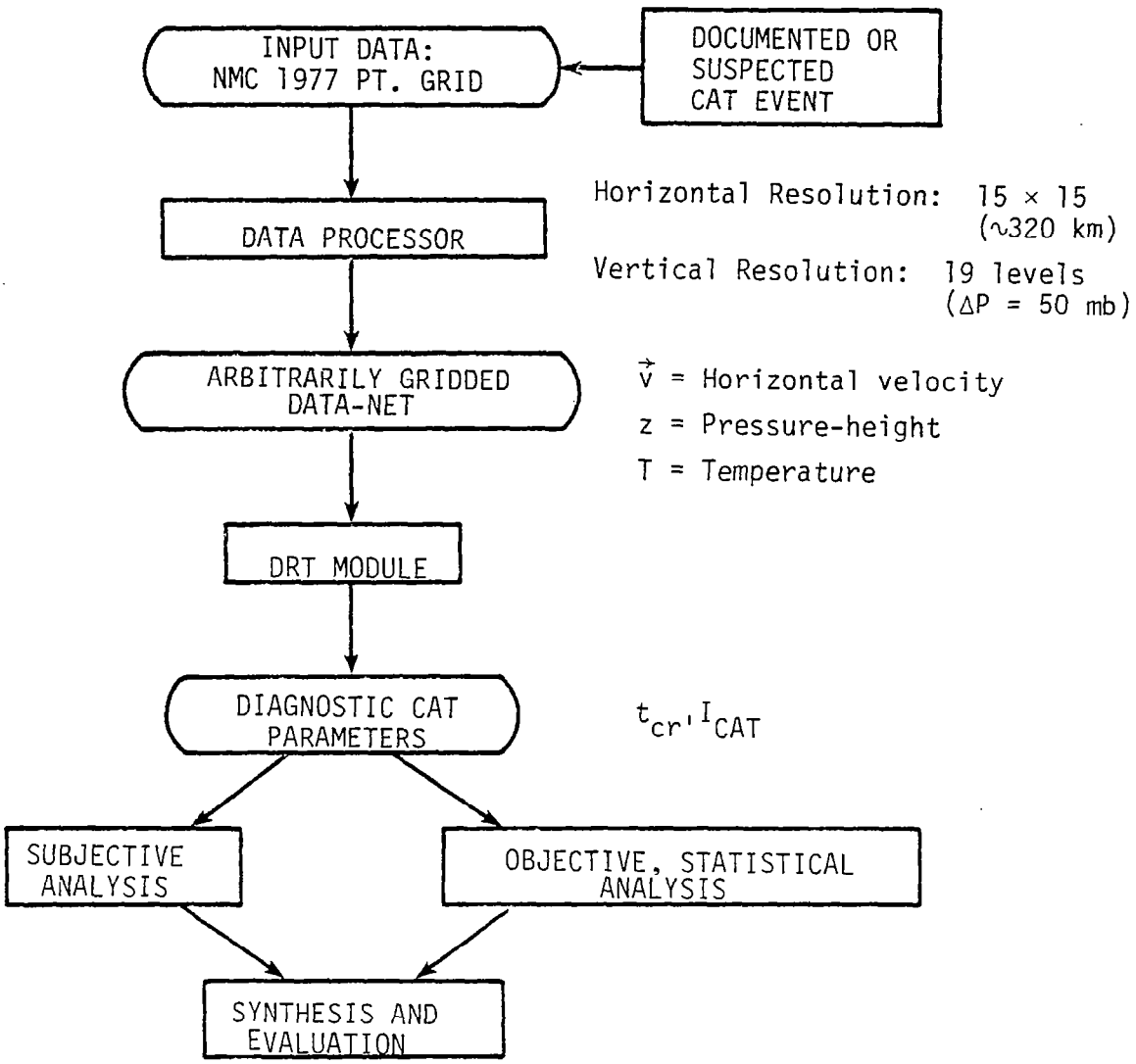

Figure 3. DRT case study methodology.

$$\Phi = \Phi(\vec{v},\ T,\ \omega_N)$$

$$\omega_{n+1} = \omega_{n+1}(T,\ \psi,\ \chi_n,\ \omega_n,\ \partial\psi/\partial t)$$

$$\omega_1 = \omega_{qg} = \omega_1(\vec{v}_g,\ z,\ \sigma_s)$$

$$\vec{v}_g = \vec{v}_g(z)$$

σ_s = constant reference atmosphere static stability

$$\psi = \psi(\vec{v})$$

$$\chi_n = \chi_n(\omega_n)$$

$$\partial\psi/\partial t = f(\omega_N,\ \psi,\ \chi_N)$$

$$t_{cr} = \ell nRi(\Phi)^{-1}$$

$$I_{CAT} = |\Delta\vec{v}|^2\,(\Phi+\phi)$$

$$\phi = 0.25 \times 10^{-5} s^{-1}$$

Figure 4. DRT Module Formulation

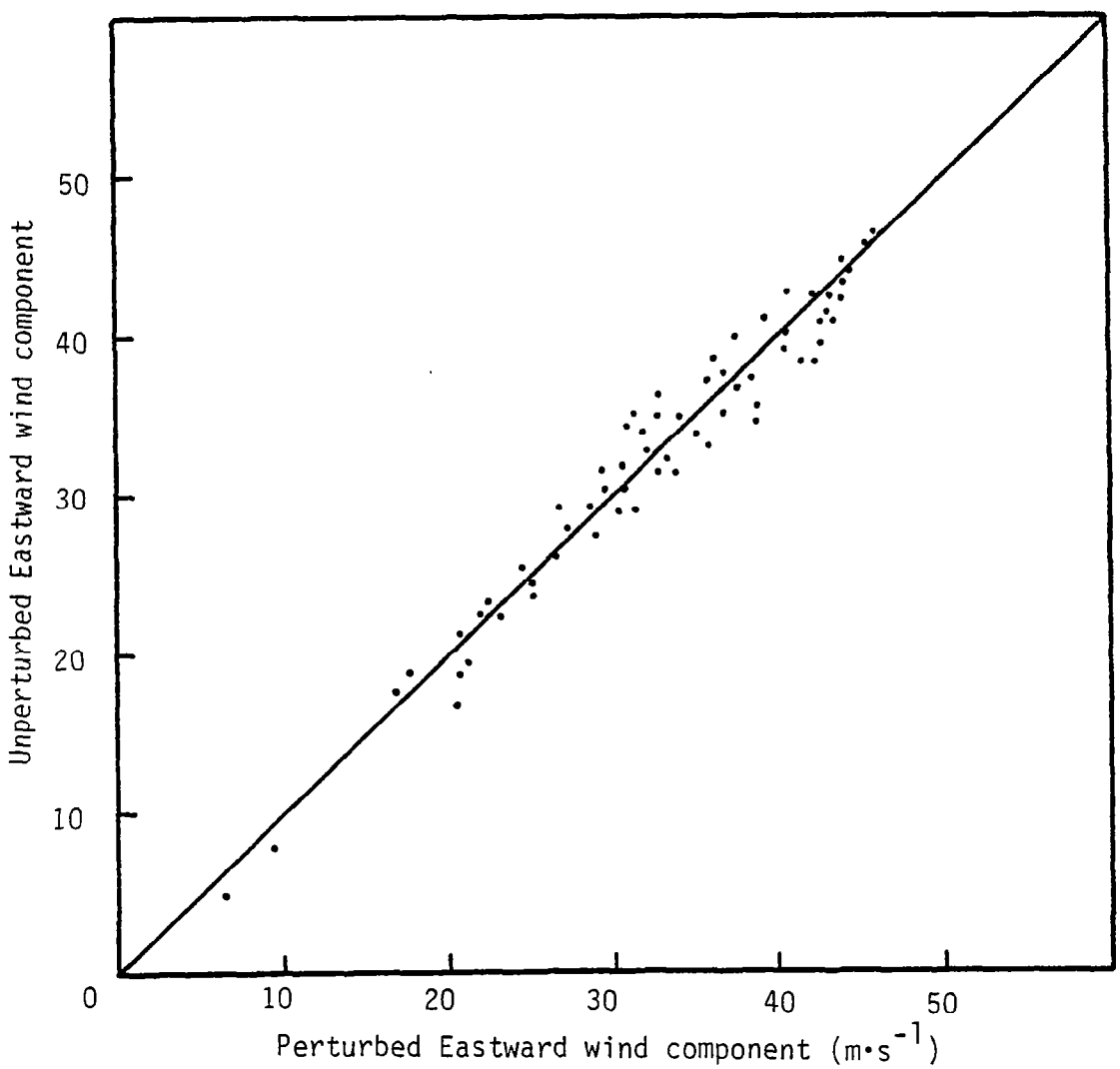

Figure 5. Scatter diagram comparing perturbed and unperturbed eastward wind components for the 500 mb pressure level.

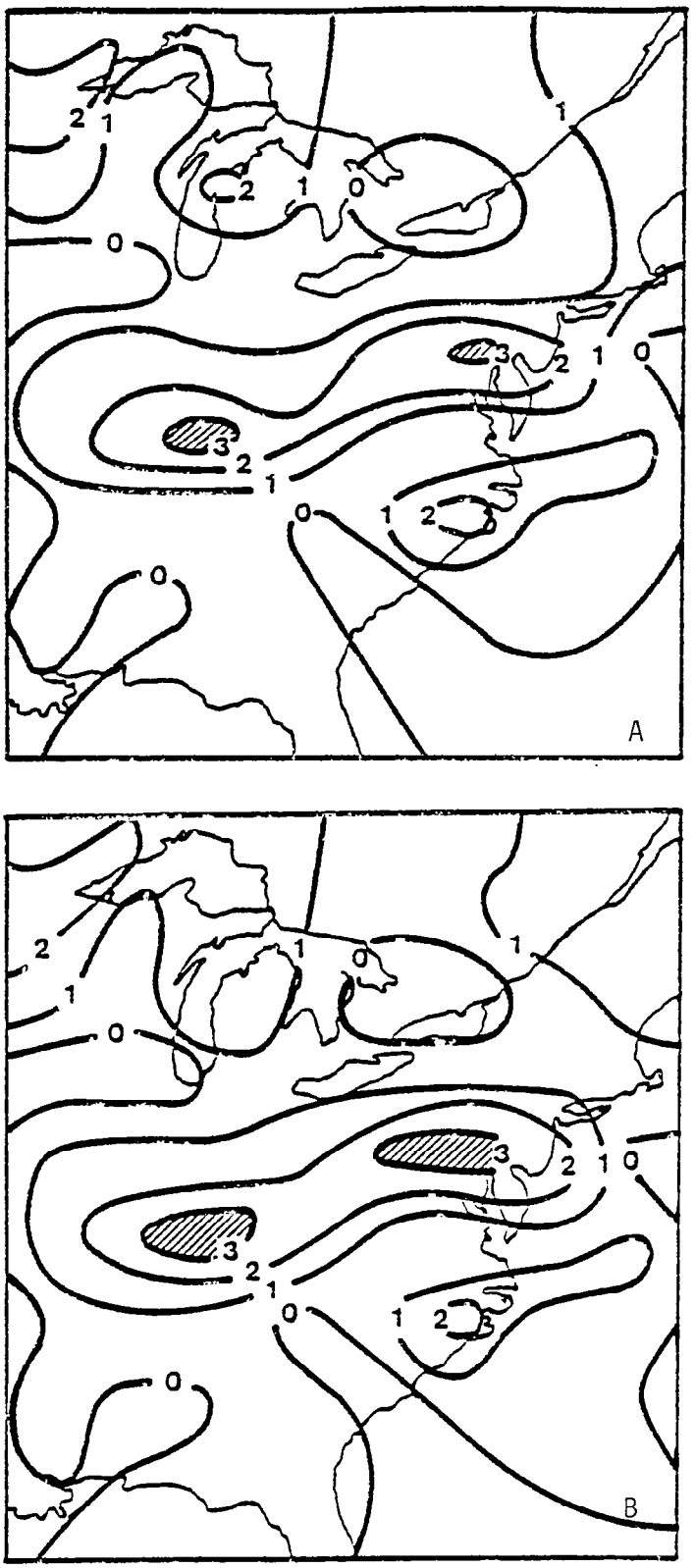

Figure 6. Vertical motion field for the (A) unperturbed and (B) perturbed wind fields at 500 mb for 0Z 20 February 1970. Units are in 10^{-1}Nt·m^{-2}·s^{-1}.

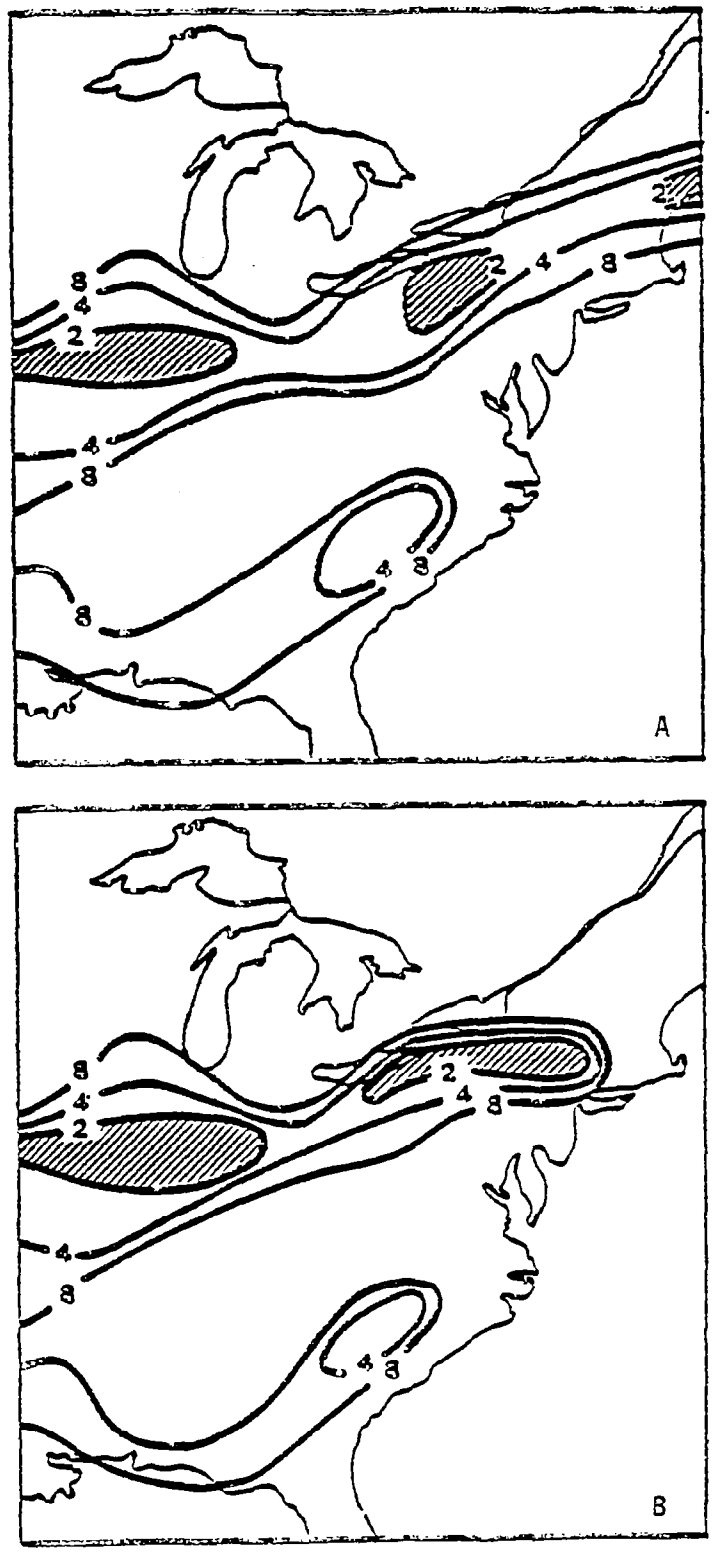

Figure 7. Time to reach Ri_{cr} for the (A) unperturbed and (B) perturbed wind fields at 500 mb for 0Z 20 February 1970 ($\times 10^4$s).

wind component that was used to assess the sensitivity of the DRT technique to errors in the horizontal wind field for the 500 mb surface of 0Z 20 February 1970. It can be seen that this component was perturbed as much as 15 percent at the 500 mb level. Other pressure-levels were similarly perturbed. Figures 6 and 7 show, respectively, the corresponding comparisons for the derived vertical motion field and t_{cr}. The hatching highlights the relative maxima of these fields. Note that except for differences in detail (notably over New England for t_{cr}) the general patterns remain the same. The significance of these results is that the DRT algorithm is relatively insensitive to reasonably small errors or inconsistencies in the input horizontal wind field. Since Φ is the primary factor calculated by the DRT algorithm, I_{CAT} must be similarly stable.

One final constraint was with respect to the vertical stratification. The vertical interpolation of temperature in the lower part of the atmosphere occasionally would result in an artificial superadiabatic lapse rate. This relatively infrequent event (generally occuring at no more than 10 percent of the points below 500 mb) results in a computational instability in the DRT algorithm. Physically, this corresponds to a negative Ri and thus a convectively unstable stratification--regardless of the degree of vertical wind shear. Turbulence associated with such layers is more characteristic of the planetary boundary layer. Since CAT of significant intensity occurs exclusively within statically stable shear layers, the main focus of consideration will be restricted to atmospheric layers which possess vertical stratification far greater than the adiabatic lapse rate. Points at which this problem occurred were simply adjusted to the adiabatic lapse rate.

RESULTS

In this study the DRT technique was applied to four case studies of pilot encounters with CAT. The results of the DRT calculations are compared to the distribution of actual encounters documented as part of a study performed by the British Central Forecast Office (CFO) published by Dutton (1979). The dates are 9 March 1976, 18 March 1976, and 24 March 1976 over the European sector of the trans-Atlantic route.

Figure 8 shows, for 0Z 9 March 1976 at the 300 mb level, lines of constant t_{cr}, in units of 10^4 seconds. Also shown are the pilot encounters (described as moderate to severe) reported near this level. The levels were chosen to show the fields of t_{cr} intersecting regions of relative maxima of CAT encounters. Because there is considerable subjectivity about the reported intensity, only those incidents described as at least "moderate" are included. The encounters are illustrated as follows: The location where CAT was initially reported is indicated by an "Encounter Letter." The location where turbulence ended is indicated by the head of an arrow. The distance over which turbulence occurred is indicated by the length of the arrow. The corresponding temporal extent is listed in the table to the right of the figure. Figure 9 illustrates the same information for 12Z. Additionally, the prognosticated regions of high CAT probability calculated by Dutton (1979) are shown by a dot-dash line and the channel of highest aircraft density by a dotted line. Dutton performed calculations for only the 12Z map times.

Figures 8 and 9 reveal that most of the moderate to severe turbulence encounters documented generally possess the characteristics usually attributed to CAT; that is, a spatial scale usually less than 100 km and temporal scales usually less than one hour. The number of encounters at the 0Z map time is small and no skill can be ascertained from Figure 8. Figure 9, however,

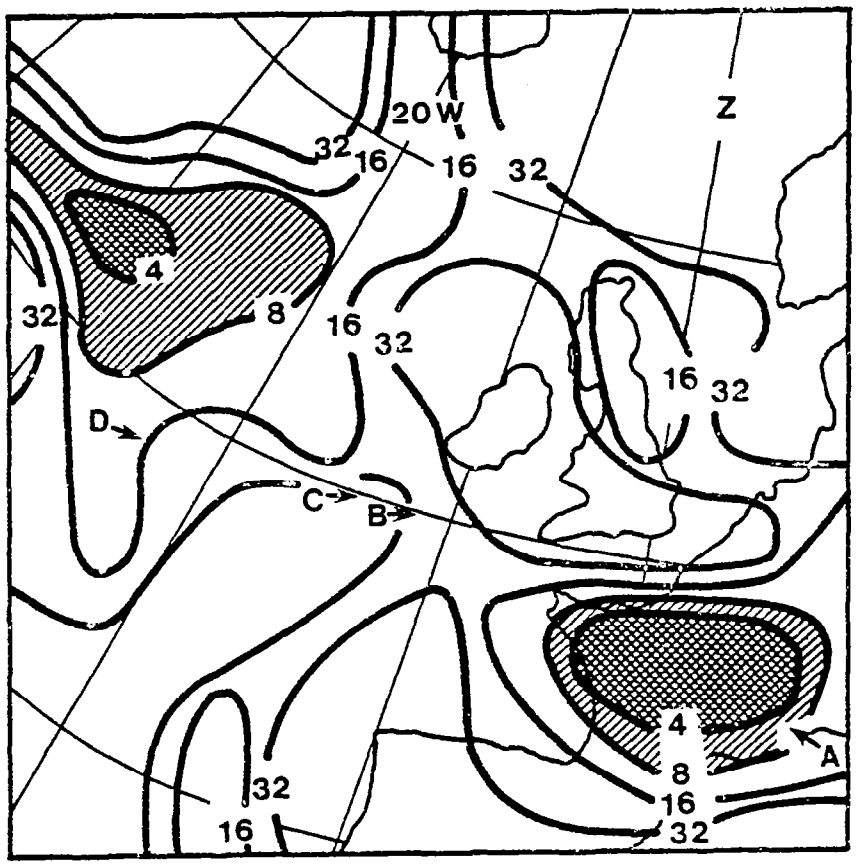

$t_{cr} \cdot 10^4$ seconds

300 mb (27 to 35,000 ft.)

ENCOUNTER/TIME

A	0315-0332Z
B	0411-0424
C	0552-0554
D	0610-0621

0Z 9 March 1976

Figure 8. Time to reach Ri_{cr} and pilot encounters with moderate to severe turbulence at 300 mb for 0Z 9 March 1976.

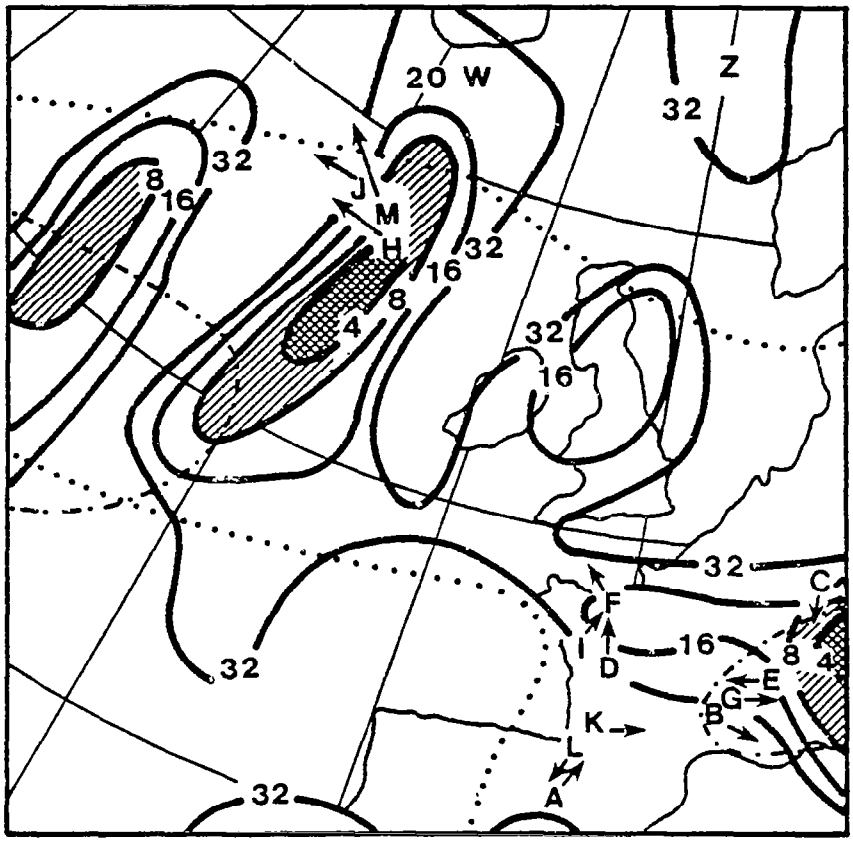

$t_{cr} \cdot 10^4$ seconds

300 mb (27 to 31,000 ft.)

ENCOUNTER	TIME
A	1033-1051Z
B	1244-1246
C	1309-1310
D	1317-1324
E	1331-1340
F	1334-1350
G	1359-1403
H	1439-1454
I	1446-1459
J	1509-1528
K	1634-1637
L	1704-1715
M	1705-1733

12Z 9 March 1976

Figure 9. Same as Figure 8, except for 12Z. The dot-dash line shows the forecast regions of CAT (Dutton, 1979); The dotted line shows the "channel" of highest aircraft density.

seems to show better results. This trend generally continues for subsequent cases, as will be shown. An alternative way to view the potential for CAT can be seen in Figure 10. A vertical cross-section of t_{cr} intersecting a hypothetical flight path at 300 mb from Rome to New York is shown. It can be seen that a pilot assigned this flight-path can expect to pass through two regions of relatively high CAT potential, over western Europe and west of Ireland.

It becomes immediately evident that the turbulence probability index supplied by the DRT formulation is much more specific and detailed than the current CAT forecast products supplied by the National Weather Service (NWS). For example, from an operational viewpoint the information shown in Figures 8 and 9 would be of even greater value. While it may not be practical to circumvent the regions of higher CAT potential, a picture of the vertical structure, as shown in Figure 10, would suggest to the pilot that the turbulence potential should be lessened by dropping only several thousand feet in altitude.

Figures 11 through 16 show the fields of t_{cr}, and CAT encounter records as well as the Dutton CAT forecast regions for the remaining three cases. In addition to information shown in previous figures, encounter letters which are circled correspond to reports of "significantly greater than moderate" turbulence.

Some of the discrepancy can perhaps be explained in considering Figures 17 and 18. These figures consist of vertical cross sections of t_{cr} along the 50°N meridian for 0Z and 12Z 18 March 1976. The CAT encounters which occurred along this corridor two to seven hours after the 0Z map time are indicated. The general eastward and downward progression of the turbulence reports appears consistent with the similar propagation in the minimum in t_{cr} initially at 11.5 km. One other feature, which is important with respect to application of the DRT technique to CAT forecasting, is the considerable degree of conservatism

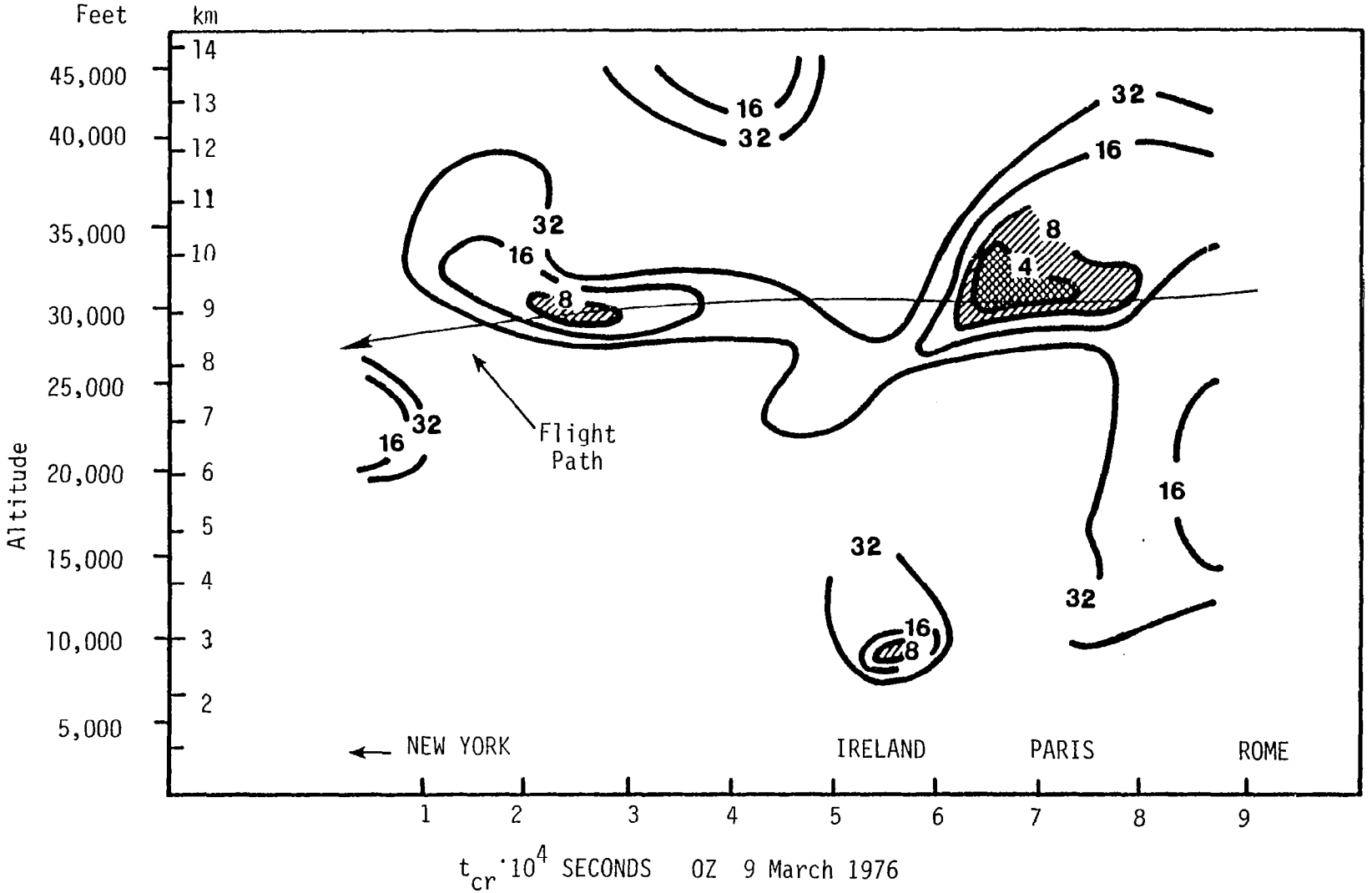

Figure 10. Hypothetical flight-path from Rome to New York at the 300 mb surface. The flight-path is shown against a vertical cross section of t_{cr}.

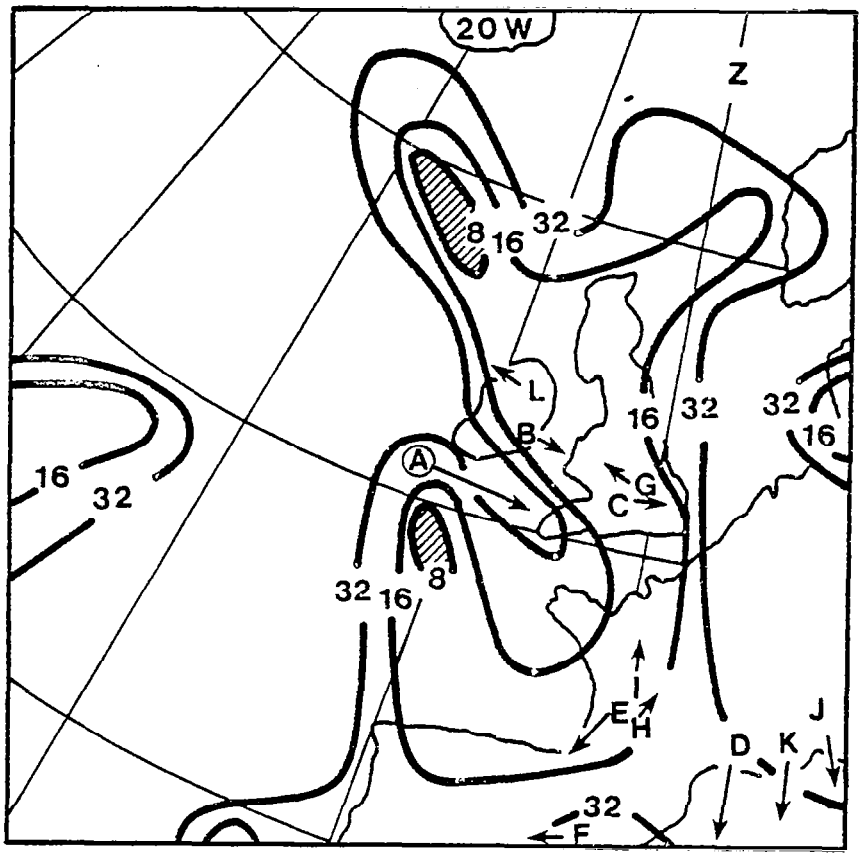

OZ 12 March 1976

$t_{cr} \cdot 10^4$ seconds

300 mb (27 to 31,000 ft.)

ENCOUNTER/TIME

A	0530-0545Z
B	0717-0729
C	0739-0800
D	0807-0821
E	0821-0840
F	0838-0846
G	0840-0850
H	0947-1004
I	1010-1013
J	1021-1037
K	1024-1038
L	1102-1105

Figure 11. Same as Figure 8, except for map time indicated.

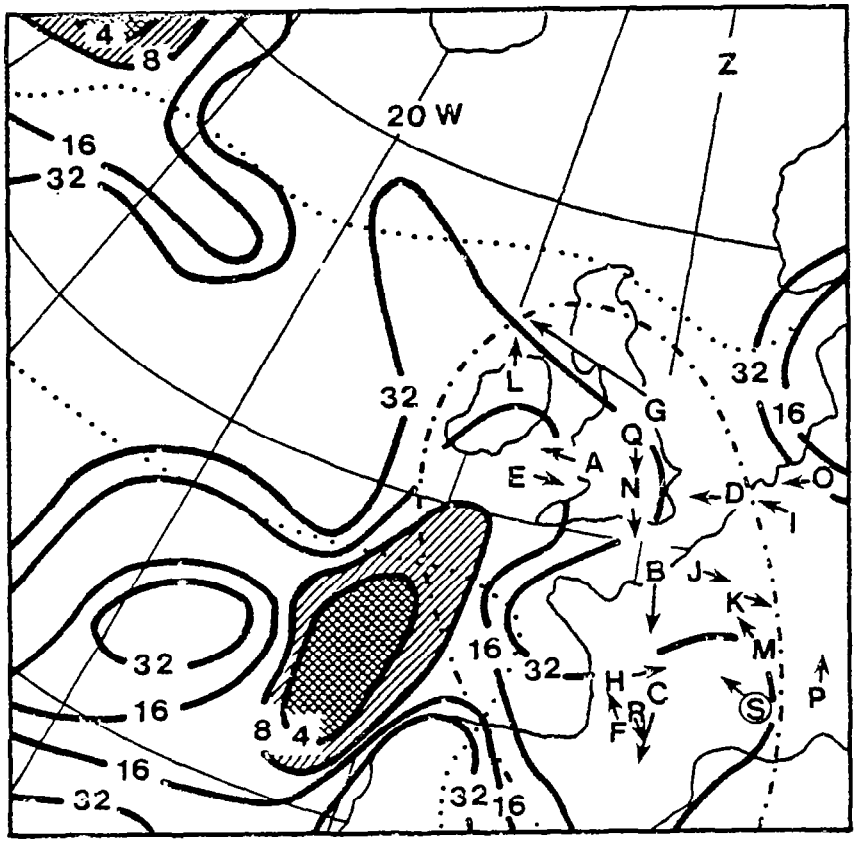

12Z 12 March 1976

$t_{cr} \cdot 10^4$ seconds

300 mb (27 to 31,000 ft.)

ENCOUNTER/TIME

A	1132-1135Z
B	1141-1152
C	1154-1210
D	1157-1201
E	1310-1314
F	1331-1351
G	1437-1519
H	1455-1509
I	1502-1510
J	1536-1548
K	1555-1605
L	1610-1612
M	1710-1727
N	1757-1811
O	1828-1830
P	1838-1850
Q	1840-1845
R	1856-1902
S	1935-1936

Figure 12. Same as Figure 9, except for map time indicated.

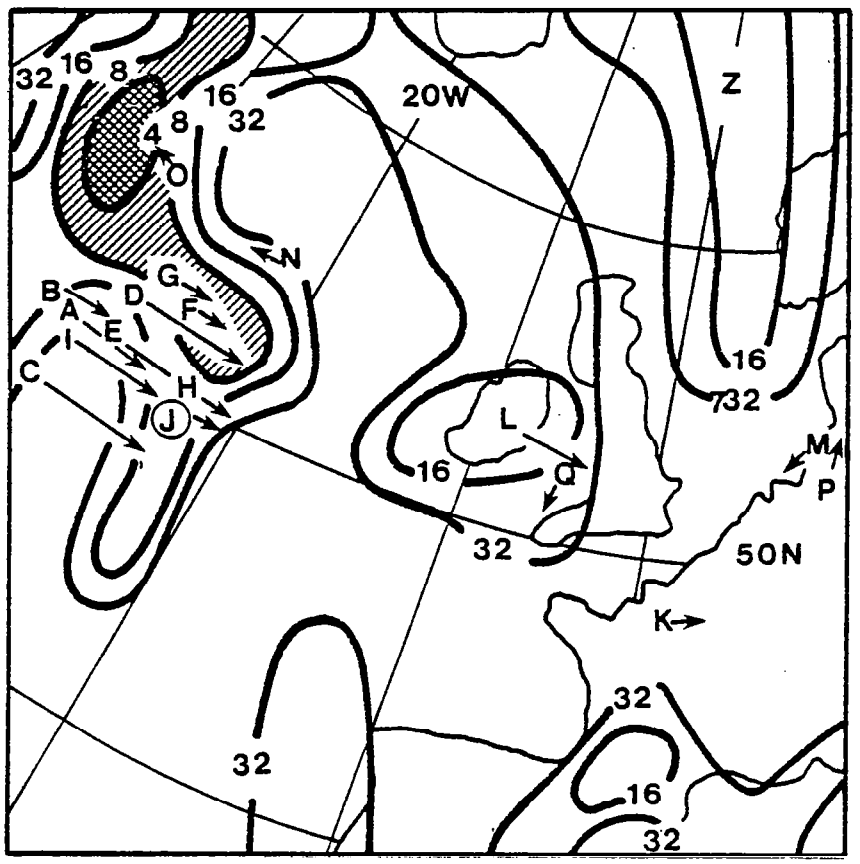

$t_{cr} \cdot 10^4$ seconds

250 mb (31 to 35,000 ft.)

ENCOUNTER/TIME

A	0220-0240Z
B	0300-0320
C	0435-0504
D	0448-0500
E	0448-0521
F	0511-0520
G	0522-0550
H	0537-0544
I	0640-0705
J	0650-0654
K	0753-0755
L	0829-0844
M	0917-0920
N	0935-0940
O	1009-1014
P	1031-1041
Q	1044-1047

0Z 18 March 1976

Figure 13. Same as Figure 8, except for map time and pressure-level indicated.

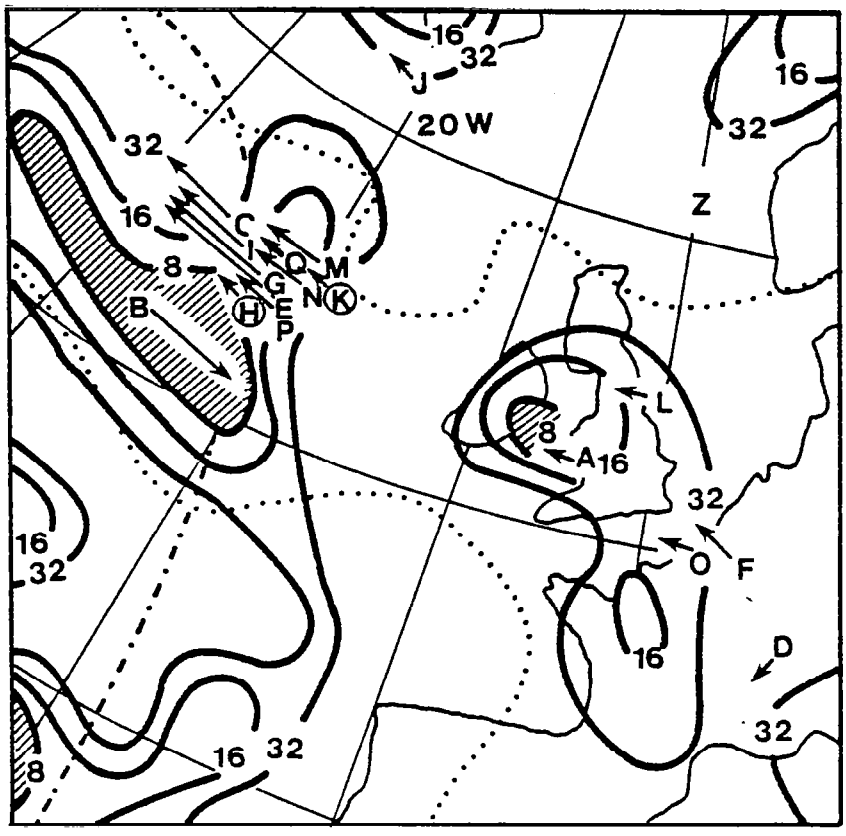

12Z 18 March 1976

$t_{cr} \cdot 10^4$ seconds

250 mb (31 to 35,000 ft.)

ENCOUNTER/TIME

A	1044-1047Z
B	1107-1131
C	1237-1306
D	1325-1335
E	1351-1434
F	1405-1419
G	1428-1458
H	1444-1502
I	1456-1521
J	1509-1511
K	1513-1530
L	1537-1545
M	1545-1621
N	1559-1659
O	1640-1650
P	1648-1703
Q	1708-1720

Figure 14. Same as Figure 9, except for map time and pressure-level indicated.

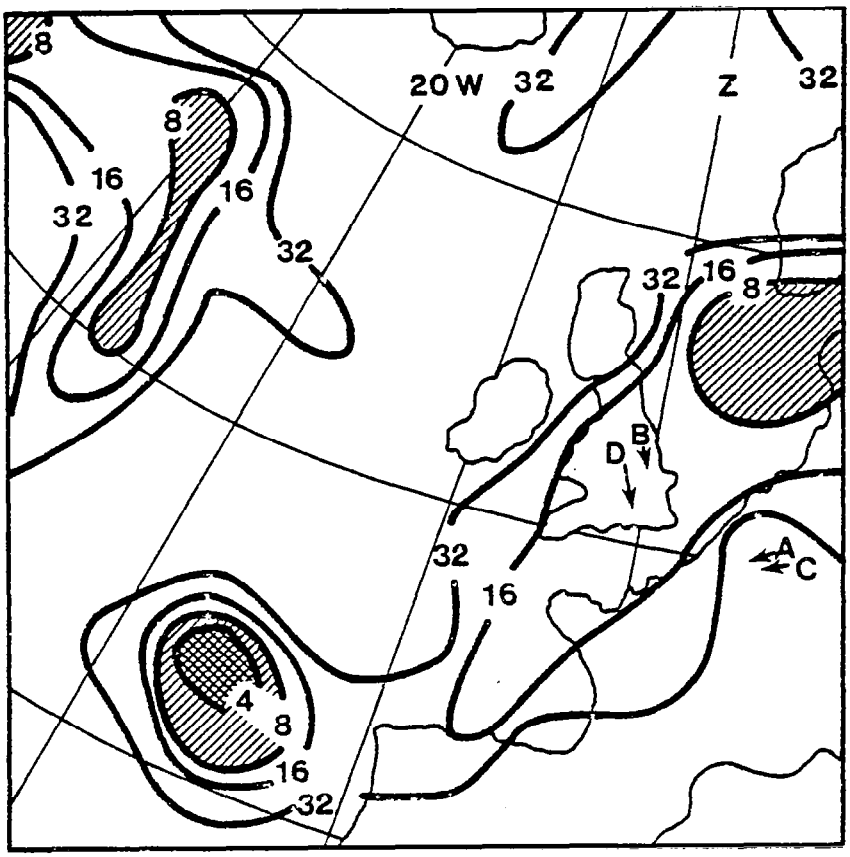

$t_{cr} \cdot 10^4$ seconds

350 mb (23 to 28,000 ft.)

ENCOUNTER/TIME

A	0725-0730Z
B	0745-0754
C	0845-0855
D	0852-0858

0Z 24 March 1976

Figure 15. Same as Figure 8, except for map time indicated.

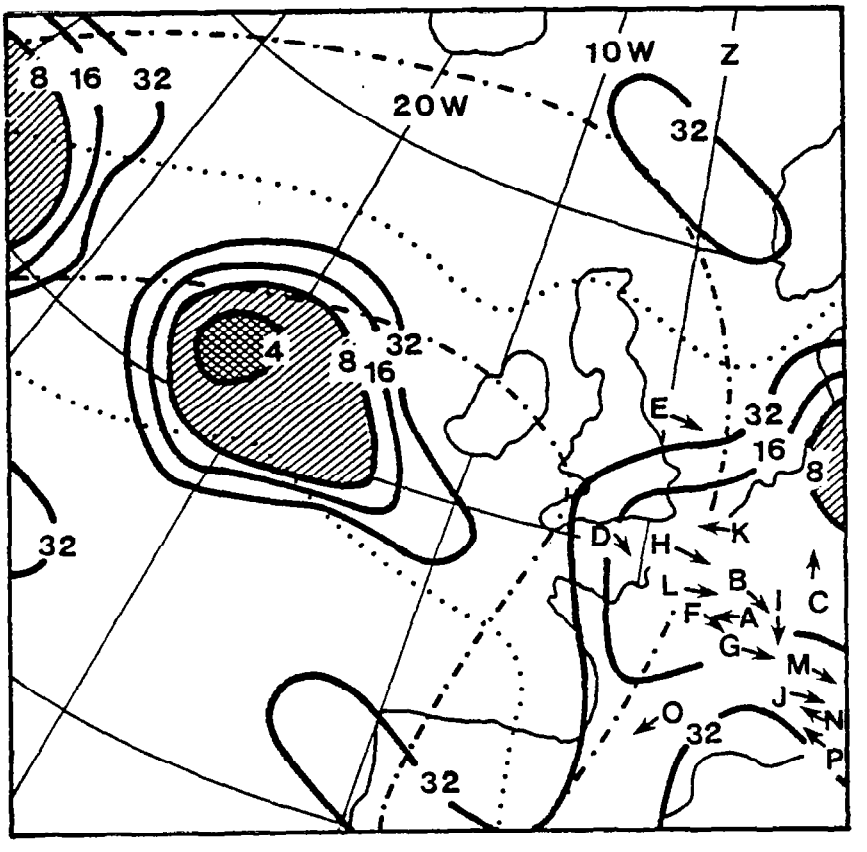

12Z 24 March 1976

$t_{cr} \cdot 10^4$ seconds

350 mb (23 to 28,000 ft.)

ENCOUNTER/TIME

A	0955-1018Z
B	1000-1005
C	1000-1010
D	1100-1105
E	1100-1111
F	1114-1124
G	1159-1205
H	1206-1216
I	1334-1335
J	1357-1404
K	1437-1442
L	1534-1540
M	1626-1629
N	1753-1756
N	1805-1809
P	1815-1826

Figure 16. Same as for Figure 9, except for map time and pressure-level indicated.

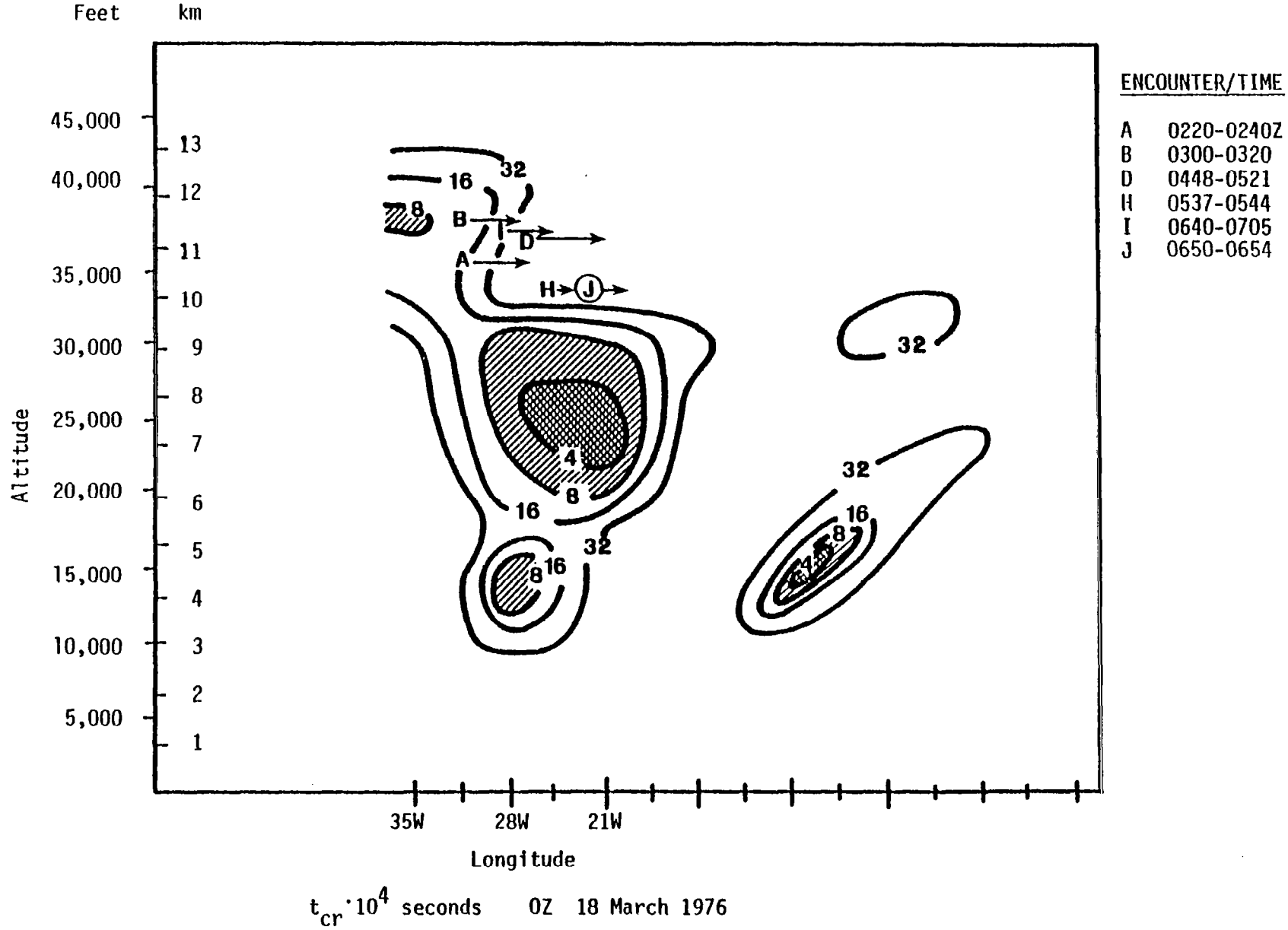

Figure 17. Vertical cross section of t_{cr} along 50^{o}N parallel.

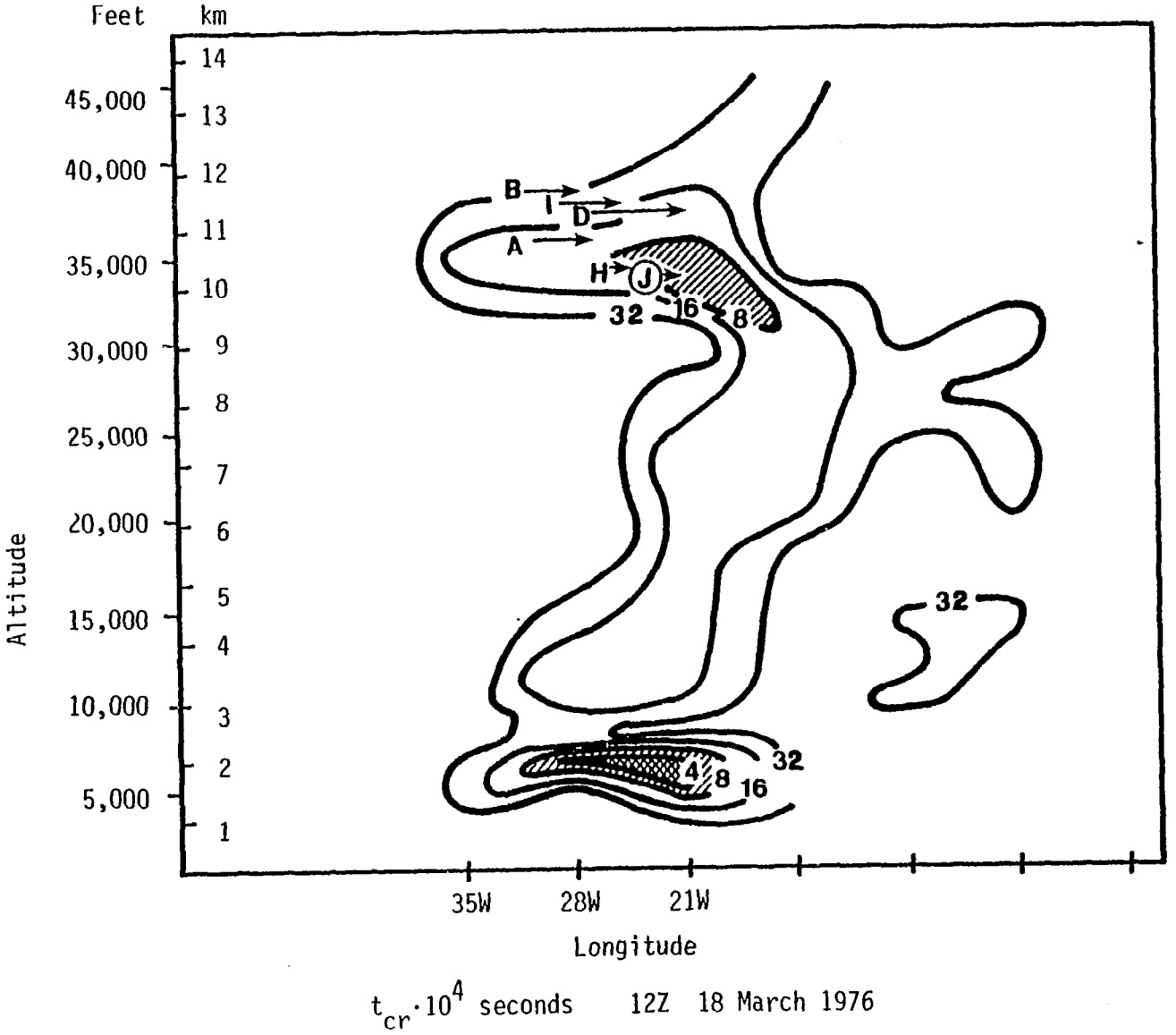

Figure 18. Same as Figure 17, except 12 hours later.

in the fields of t_{cr}. Indeed, it may be possible, for relatively short forecast periods, to construct a prognostic scheme, analogous to the absolute vorticity conserving barotropic models used as early weather prediction models, where t_{cr} would simply be advected by the three-dimensional wind field.

As discussed in the second section, there is reason to believe that including the magnitude of the vertical shear in a DRT-based CAT potential index would improve its performance. Hence, yet another way to improve the agreement between CAT encounters and their proximity to source regions might be use of a more physically realistic index.

Consider Figure 19. This figure shows the pressure-heights (solid lines) and isotachs (dashed lines) for 0Z 18 March 1976 at 250 mb. The isotachs are in units of $m \cdot s^{-1}$ and the heights in decameters. Shaded areas delineate regions of highest wind velocity. The direction will generally parallel the lines of constant height. Comparison with Figure 13 reveals that a minimum in t_{cr} exists just west of 25 W longitude. This center is mainly north and west of a very strong wind maximum ($60\ m \cdot s^{-1}$). How this translates into the CAT potential index defined by Eq. (9) is seen in Figures 20 and 21. The index I_{CAT} is constructed so that larger values correspond to higher potential. Although a source region, related to the minimum in t_{cr}, is shown positioned closer to the reported encounters, Figure 21 reveals an even more interesting event. It can be seen that between 0Z and 12Z, the area of I_{CAT} intensified at this level. Observational confirmation of this intensification is strongly suggested by the report of "considerably greater than moderate turbulence" designated as encounter "J" which had the latest time for the initiation of its encounter at this latitude.

Further analysis is needed to determine whether this apparent intensification in I_{CAT} implies that this index is not as conservative as is t_{cr}. Indeed, the degree of conservatism

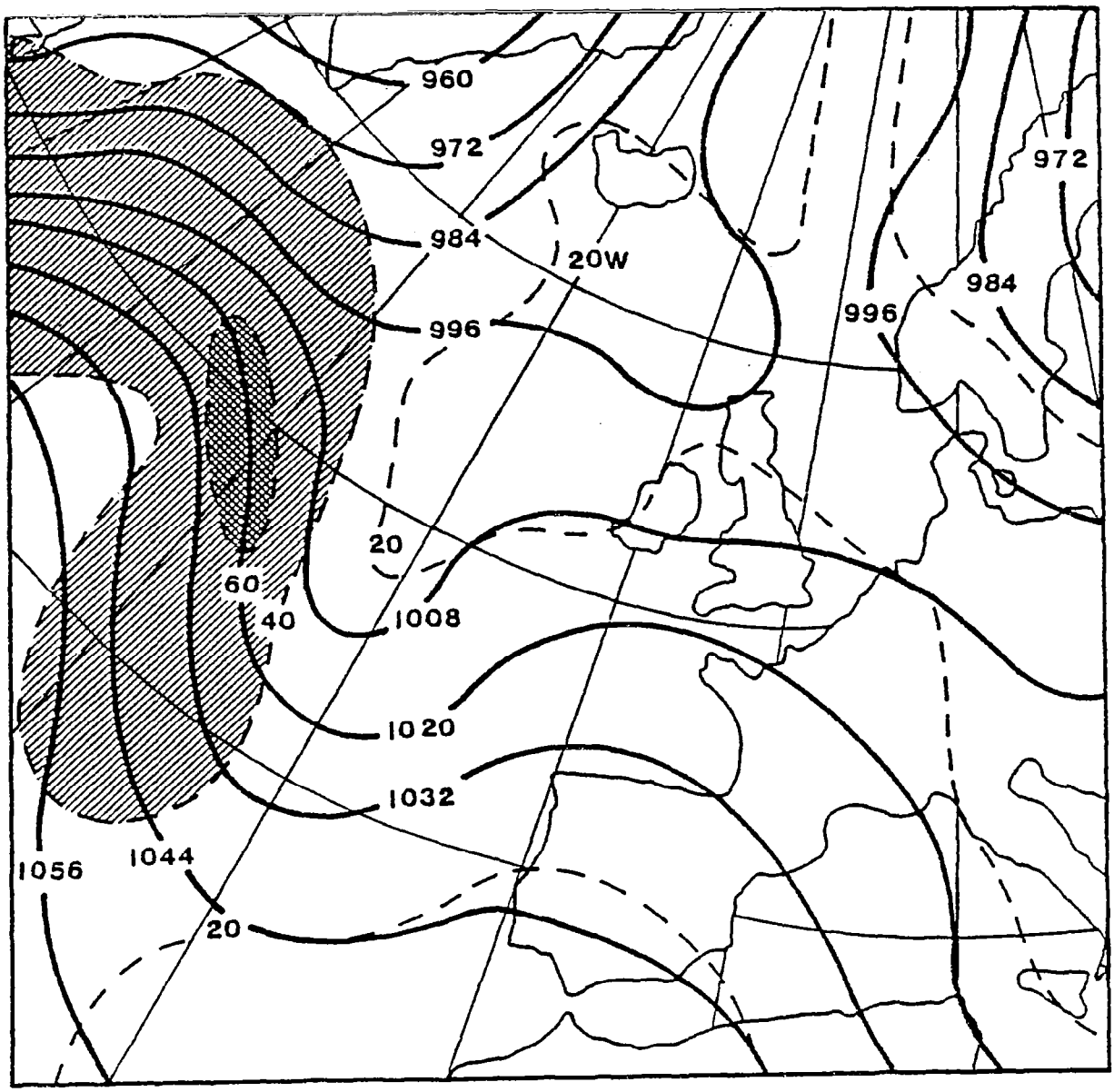

0Z 18 March 1976

Figure 19. Pressure heights, in decameters (solid lines), and Isotachs ($m \cdot s^{-1}$) (dashed lines), at 250 mb.

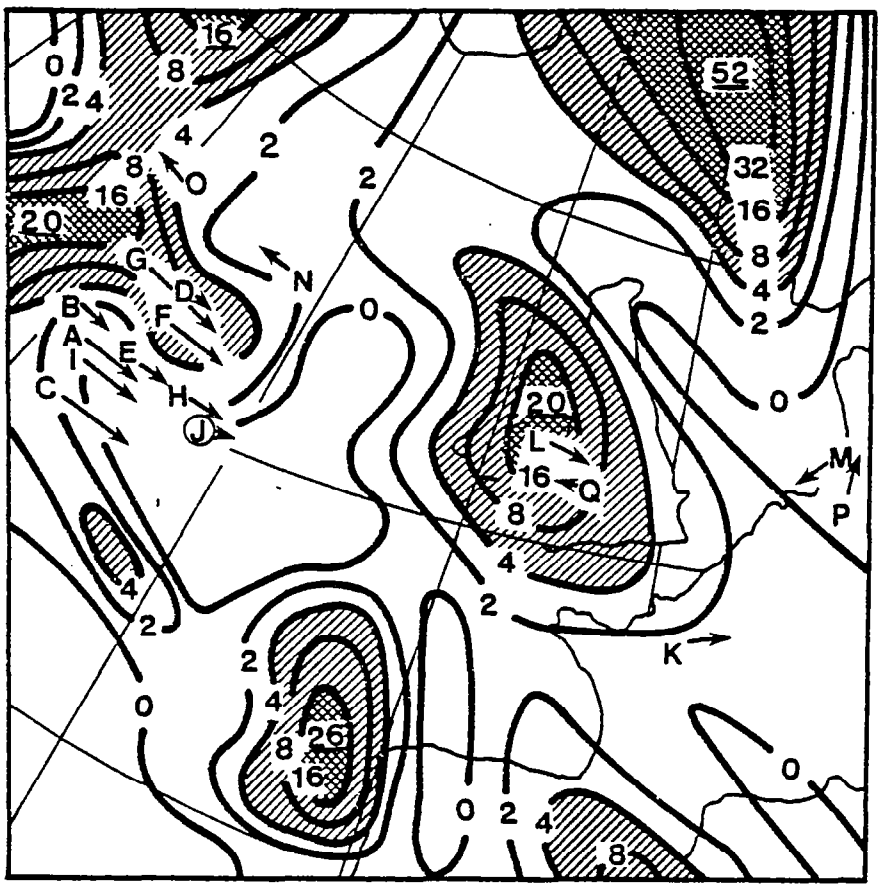

$I_{CAT}(cm^2 \cdot s^{-2})s^{-1}$

250 mb (31 to 35,000 ft.)

ENCOUNTER/TIME

A	0220-0240Z
B	0300-0320
C	0435-0504
D	0448-0500
E	0448-0521
F	0511-0520
G	0522-0550
H	0537-0544
I	0640-0705
J	0650-0654
K	0753-0755
L	0829-0844
M	0917-0920
N	0935-0940
O	1009-1014
P	1031-1041
Q	1044-1047

OZ 18 March 1976

Figure 20. CAT potential index for the 4000 foot interval centered at 250 mb, and pilot encounters with moderate to severe turbulence. Maximum values of I_{CAT} are indicated by underlining.

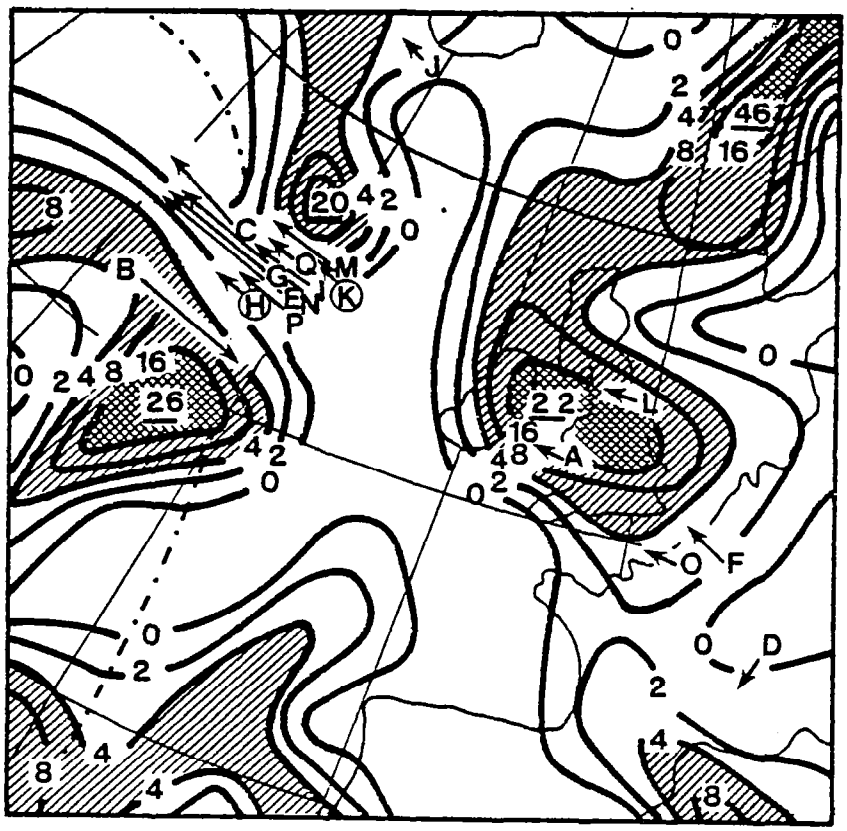

$I_{CAT}(cm^2 \cdot s^{-2})s^{-1}$

250 mb (27 to 31,000 ft.)

ENCOUNTER/TIME

A	1044-1047Z
B	1107-1131
C	1237-1306
D	1325-1335
E	1351-1434
F	1405-1419
G	1428-1458
H	1444-1502
I	1456-1521
J	1509-1511
K	1513-1530
L	1537-1545
M	1545-1621
N	1559-1659
N	1640-1650
O	1640-1650
P	1648-1703
Q	1708-1720

12Z 18 March 1976

Figure 21. Same as Figure 20, except for map time and pressure-level indicated.

of t_{cr} itself is speculative at this time. Important elements to be considered in this regard include the relative roles played by advective versus the actual amplification processes.

Figures 22 through 27 show the fields of I_{CAT} and CAT encounters for the other three cases. In general this index appears to be superior to t_{cr} for specifying potential regions of CAT. In particular, that for 0Z 9 March 1976 (Figure 22) reveals clearly why there were few encounters of CAT during this time. While Figure 8 indicates very small values of t_{cr} over Europe for this time, the corresponding I_{CAT} field shows generally small values of I_{CAT}. Hence it can be concluded that although CAT may have occurred associated with the small t_{cr} values, it was of weak intensity.

A more quantitative comparison is shown in Figure 28, which summarizes the CAT encounters in relation to the "centers of action" responsible for their existence. For example, 85 percent of the encounters were reported in regions where $I_{CAT} > 0$, 57 percent for $I_{CAT} > 2(cm^2 \cdot s^{-2})s^{-1}$. Similarly, 73 percent of the encounters occurred when $t_{cr} < 32 \times 10^4 s$. It can be seen that I_{CAT} is apparently a more accurate indicator of CAT potential.

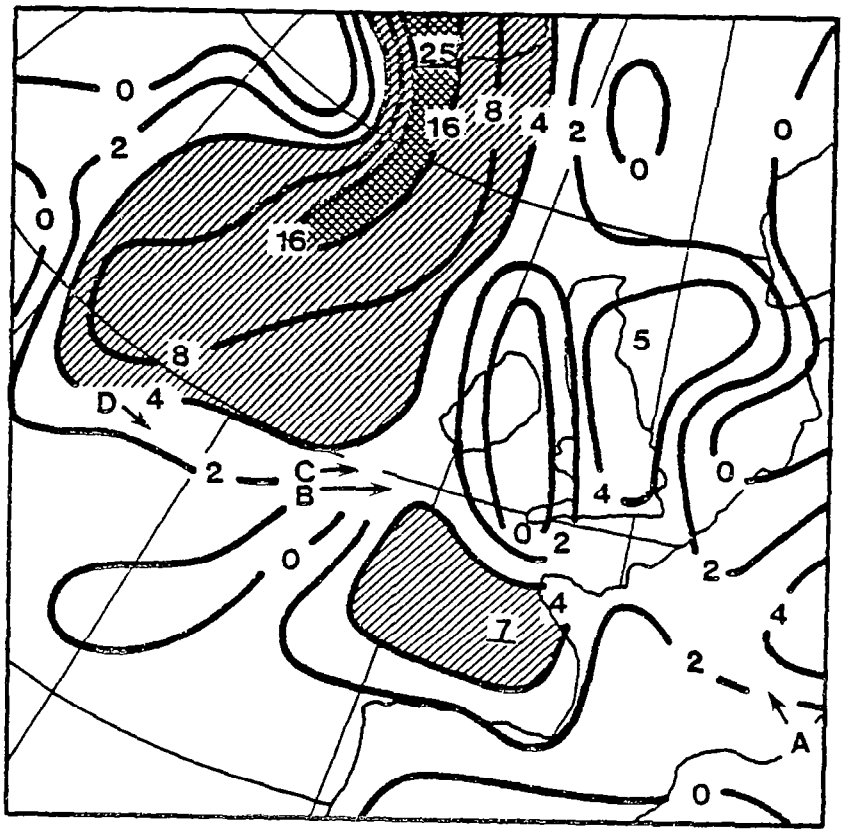

OZ 9 March 1976

$I_{CAT}(cm^2 \cdot s^{-2})s^{-1}$

300 mb (27 to 31,000 ft.)

ENCOUNTER/TIME

A	0315-0332Z
B	0411-0424
C	0552-0554
D	0610-0621

Figure 22. CAT potential index, I_{CAT}, and pilot encounters with moderate to severe turbulence at 300 mb for OZ 9 March 1976.

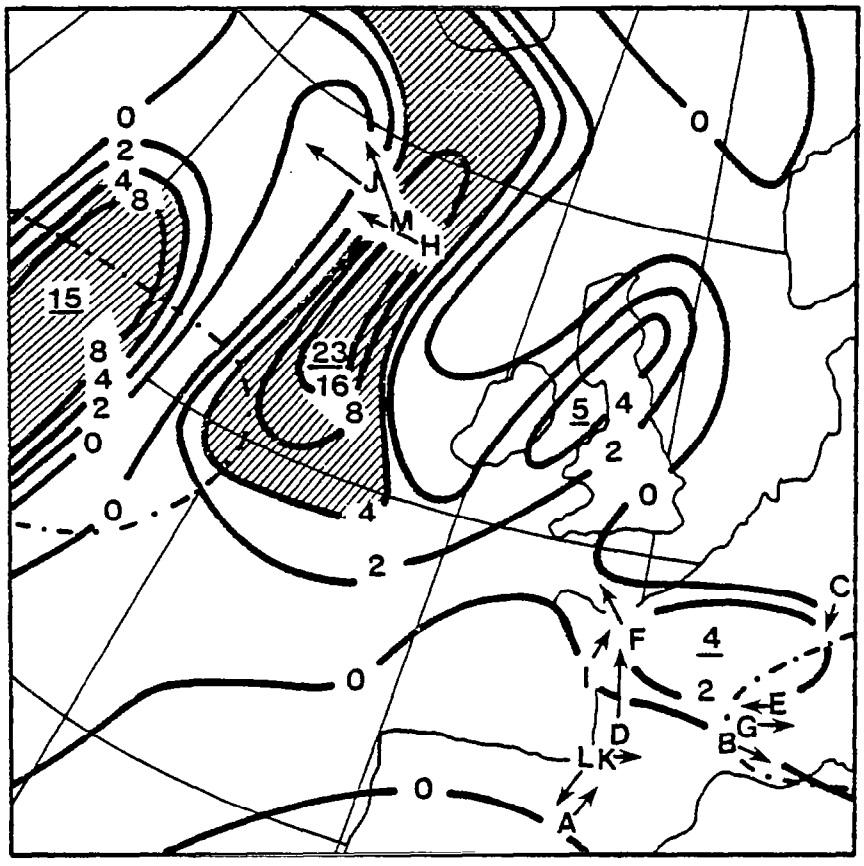

$I_{CAT}(cm^2 \cdot s^{-2})s^{-1}$

300 mb (27 to 31,000 ft.)

ENCOUNTER/TIME

A	1033-1051Z
B	1244-1246
C	1309-1310
D	1317-1324
E	1331-1340
F	1334-1350
G	1359-1403
H	1439-1454
I	1446-1459
J	1509-1528
K	1634-1637
L	1704-1715
M	1705-1733

12Z 9 March 1976

Figure 23. Same as Figure 22, except for 12Z

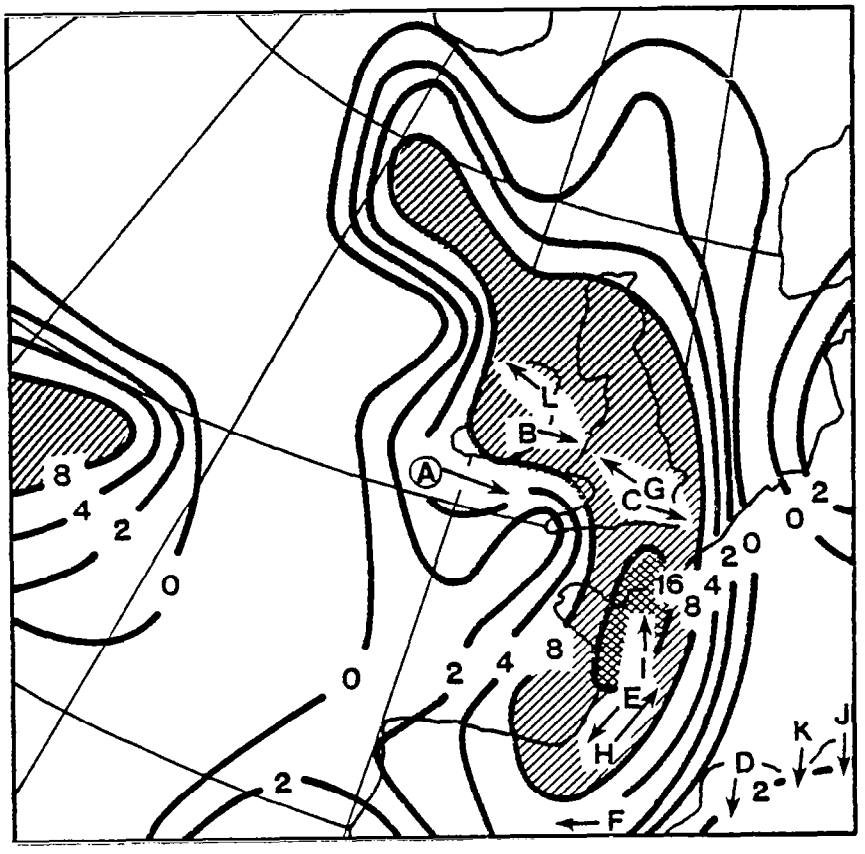

OZ 12 March 1976

$I_{CAT}(cm^2 \cdot s^{-2})s^{-1}$

300 mb (27 to 31,000 ft.)

ENCOUNTER/TIME

A	0530-0545Z
B	0717-0729
C	0739-0800
D	0807-0821
E	0821-0840
F	0838-0846
G	0840-0850
H	0947-1004
I	1010-1013
J	1021-1037
K	1024-1038
L	1102-1105

Figure 24. Same as Figure 22, except for map time indicated.

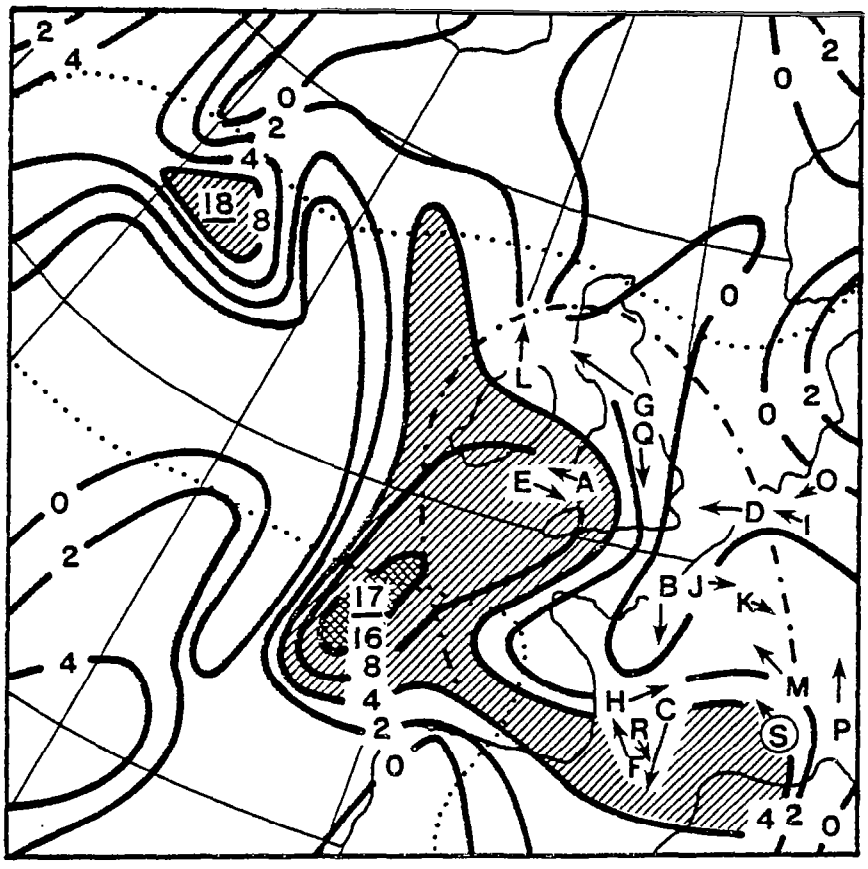

$I_{CAT}(cm^2 \cdot s^{-2})s^{-1}$

350 mb (27 to 31,000 ft.)

ENCOUNTER/TIME

A	1132-1135Z
B	1141-1152
C	1154-1210
D	1157-1201
E	1310-1314
F	1331-1351
G	1437-1519
H	1455-1509
I	1502-1510
J	1536-1548
K	1555-1605
L	1610-1612
M	1710-1727
N	1757-1811
O	1828-1830
P	1838-1850
Q	1840-1845
R	1856-1902
S	1935-1936

12Z 12 March 1976

Figure 25. Same as Figure 23, except for map time indicated.

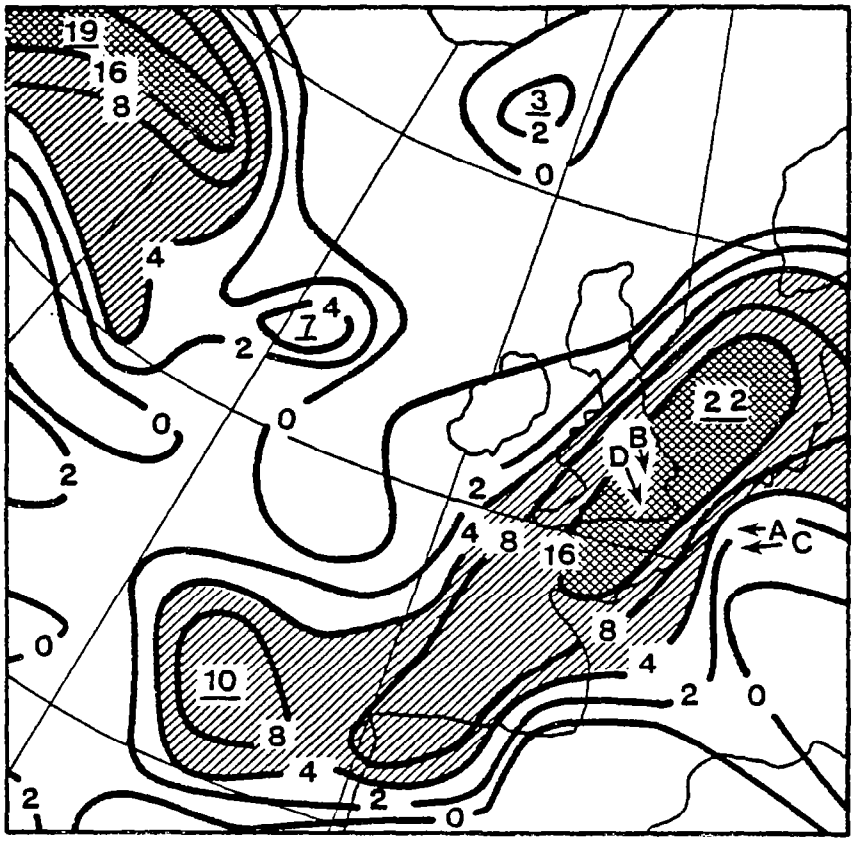

0Z 24 March 1976

$I_{CAT}(cm^2 \cdot s^{-2})s^{-1}$

350 mb (23 to 28,000 ft.)

ENCOUNTER/TIME

A	0725-0730Z
B	0745-0754
C	0845-0855
D	0852-0858

Figure 26. Same as Figure 22, except for map time indicated.

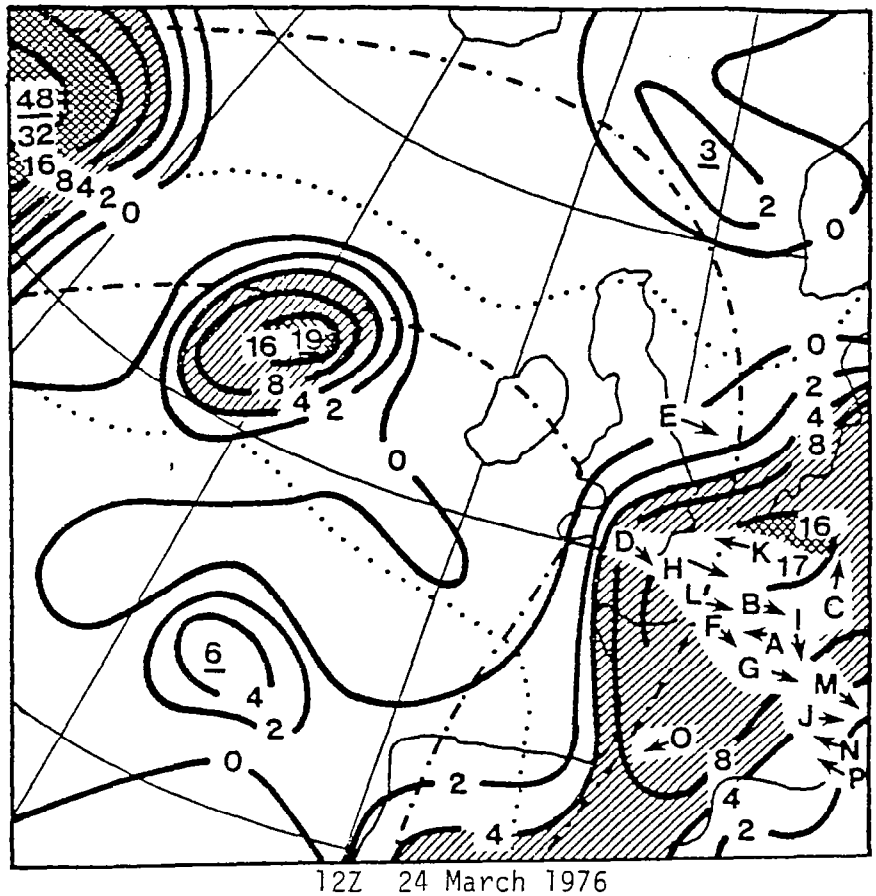

12Z 24 March 1976

$I_{CAT}(cm^2 \cdot s^{-2})s^{-1}$

350 mb (23 to 28,000 ft.)

ENCOUNTER/TIME

A	0955-1018Z
B	1000-1005
C	1000-1010
D	1100-1105
E	1100-1111
F	1114-1124
G	1159-1205
H	1206-1216
I	1334-1335
J	1357-1404
K	1437-1442
L	1534-1540
M	1626-1629
N	1753-1756
O	1805-1809
P	1815-1826

Figure 27. Same as for Figure 23, except for map time indicated.

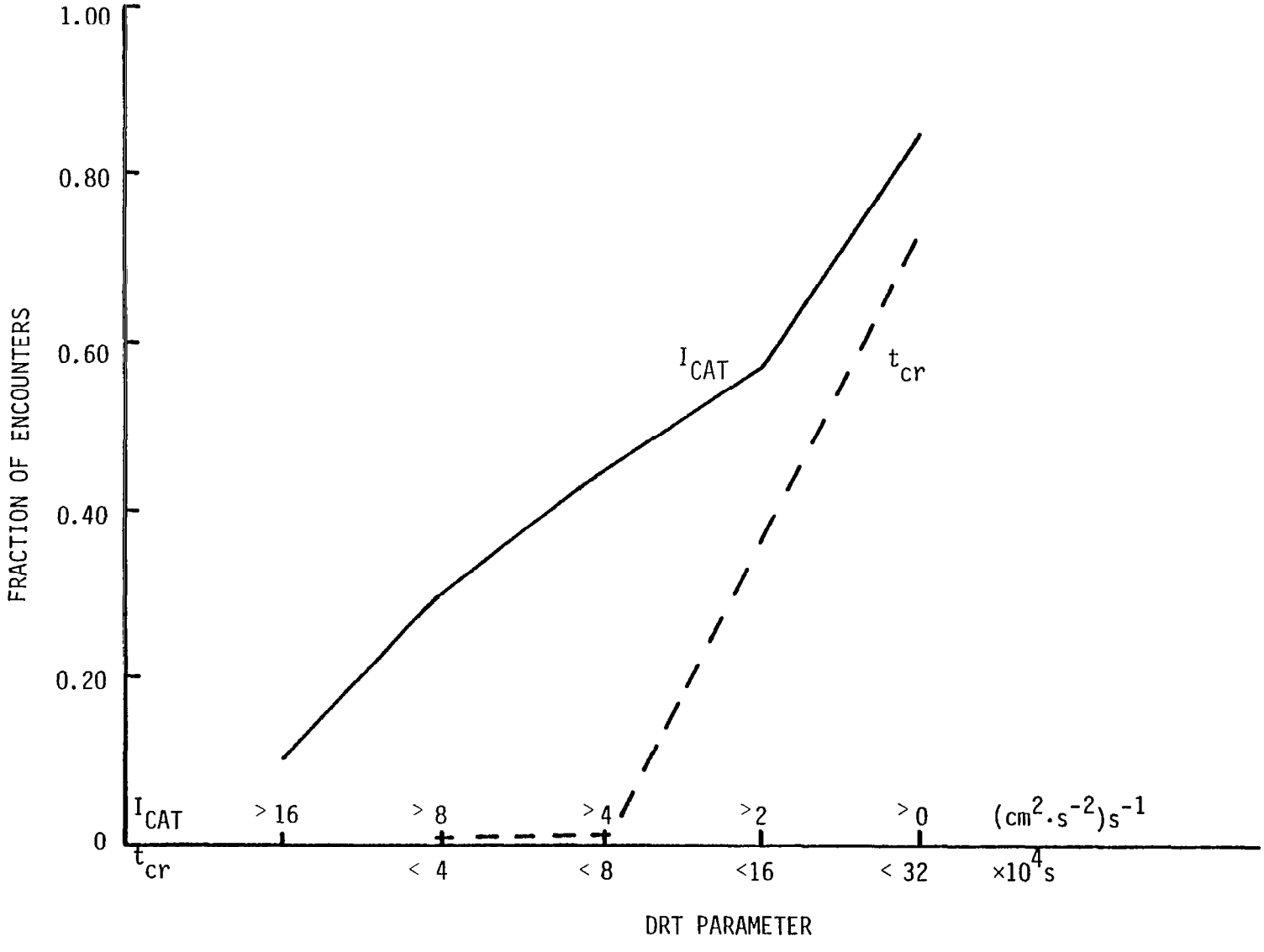

Figure 28. Fraction of reported encounters as a function of CAT potential parameters t_{cr} and I_{CAT} for all cases.

SUMMARY AND DISCUSSION

The results of several case studies of clear air turbulence (CAT) using the Diagnostic Richardson number Tendency (DRT) formulation have been highlighted. The performance of this technique in resolving regions of documented CAT encounters was encouraging. An attractive aspect of its operational adaptability is that the input data can be supplied by the currently operational Rawinsonde system.

Two indices are calculated deterministically from the synoptic-scale changes in static stability and vertical wind shear conducive for supporting meso-scale CAT layers. The products generated by the DRT formulation highlight specific regions of the atmosphere which could be interpreted operationally in terms of a CAT-encounter probability. The apparent improvement inherent in the index I_{CAT} can be argued in the course of comparing the t_{cr} fields for the 18 March 1976 case with the I_{CAT} fields for this case. The low t_{cr} region under consideration shows an eastward and southward progression at this level, but the values of t_{cr} actually increased (Figures 13 and 14). This might lead to an interpretation of decreasing CAT activity. The fields of I_{CAT} illustrated in Figures 20 and 21 imply both a south-eastward propagation and general increase in CAT activity and intensity. Pilot reports of CAT suggest that the patches of CAT generated by this region increased in number and intensity. Of course, further detailed investigations are required to establish the definite advantage of I_{CAT}.

The availability of archived data of twice the horizontal resolution used in this study suggests that the DRT technique be tested on post-July 1978 encounters. This could be done in conjunction with an improved method for vertical interpolation of the horizontal wind field. A further refinement would be to include a parameterization for the effects of significant terrain at the lower boundary. Thus, the generally higher

frequency of turbulence observed above and downwind of mountainous regions could be accounted for.

Pursuing the DRT technique further through more detailed quantitative analyses of CAT case studies and refinements in the algorithm seems justifiable. Such a conclusion is based upon the encouraging results presented here as well as the motivations related to passenger comfort and safety, and reduction in fuel consumption.

REFERENCES

Bevington, P. R., 1969: Data Reduction and Error Analysis for the Physical Sciences, New York, McGraw-Hill, 259-265.

Bretherton, F. P., 1969: "Momentum Transport by Gravity Waves," Quart. J. Roy. Meteor. Soc., 95(404), 213-243.

Burridge, D. M., and A. J. Gadd, 1977: "The Meteorological Office Operational 10-Level Numerical Weather Prediction Model," Sci. paper, Meteor. Off., No. 34.

Camp, D. W., and F. E. Caplan, 1969: "High Resolution Balloonborne Temperature Sensor," J. Appl. Meteor., 8(1), 259-166.

Camp, D. W., and W. Frost, 1980: "Fourth Annual Workshop on Meteorological and Environmental Inputs to Aviation Systems," Rebecca A. Durocher, editor. FAA report in preparation.

Dutton, M. J. O., 1979: "Performance of Conventional Operational Forecasts of Clear-Air Turbulence During the 1976 Turbulence Survey," The Meteorological Magazine, 108, 61-76.

Essenwanger, O. M., and E. R. Reiter, 1969: "Power Spectrum, Structure Function, Vertical Wind Shear, and Turbulence in Troposphere and Stratosphere," Arch. Met. Geoph. Biokl., Ser. A., 18, 17-24.

Fichtl, G. H., 1971: "The Responses of Rising or Falling Spherical Wind Sensors to Atmospheric Wind Perturbations," J. Appl. Meteor., 10(6), 1275-1284.

Gary, B. L., 1980: JPL-NASA, personal communication.

Haines, P., 1980: Report in progress.

Haltiner, G. L., and F. L. Martin, 1957: Dynamical and Physical Meteorology, New York, McGraw-Hill, 287-289.

Hines, C. O., 1968: "Some Consequences of Gravity-Wave Critical Layers in the Upper Atmosphere," J. Atmos. and Terres. Phys., 30, 837-843.

Jordan, A. R., 1972: "Atmospheric Gravity Waves from Winds and Storms," J. Atm. Sci. 29(3), 445-456.

Keller, J. L., 1978: "Prediction and Monitoring of Clear Air Turbulence: An Evaluation of the Applicability of the Rawinsonde System," NASA CR-3072.

Keller, J. L., P. A. Haines, and J. K. Luers, November 1979: "The Diagnostic Richardson Number Tendency as an Index of Clear Air Turbulence Potential," WMO Technical Conference on Aviation Meteorology, TECAM-32, Geneva, Switzerland.

Lalas, D. P., F. Einaudi, and D. Fua, 1976: "The Destabilizing Effect of the Ground on Kelvin-Helmholtz Waves in the Atmosphere," J. Atm. Sci., 33(1), 59-69.

Lalas, D. P., and F. Einaudi, 1976: "On the Characteristics of Gravity Waves Generated by Atmospheric Shear Layers," J. Atm. Sci., 33(7), 1248-1259.

Lindzen, R. S., 1974: "Stability of a Helmholtz Velocity Profile in a Continuously Stratified, Infinite Boussinesq of Fluid-Applications to Clear Air Turbulence," J. Atm. Sci., 31(6), 1507-1514.

Lindzen, R. S., and A. J. Rosenthal, 1976: "On the Instability of Helmholtz Velocity Profiles in Stably Stratified Fluids When a Lower Boundary is Present," J. Geophys. Res., 81(9), 1561-1571.

Luers, J. K., and C. D. MacArthur, 1975: "Optimum Radars and Filters for the Passive Sphere System," NASA-CR-111952.

Miles, J. W., and L. N. Howard, 1964: "Note on a Heteorogeneous Shear Flow," J. Fluid Mech., 20, 331-336.

Oard, M. J., 1974: "Application of a Diagnostic Richardson Number Tendency to a Case Study of CAT," J. Appl. Meteor., 13(7), 771-777.

Pinus, N. Z., 1964: "Atmospheric Turbulence," NASA TT F-246.

Range Commanders Council Document 110-77, 1977: Committee of the Meteorological Group, Secretariat Range Commanders Council, White Sands Missile Range, New Mexico, 19pp.

Reed, R. J., and K. R. Hardy, 1972: "A Case Study of Persistent Intense Clear Air Turbulence in an Upper Level Frontal Zone," J. Appl. Meteor., 11(3), 541-549.

Reiter, E. R., 1969: "The Nature of Clear Air Turbulence: A Review;" in Clear Air Turbulence and Its Detection, Y. Pao and A. Goldburg, editors, New York, Plenum Press, 7-33.

Roach, W. T., 1970: "On the Influence of Synoptic Development on the Production of High Level Turbulence," Quart. J. Roy. Meteor. Soc., 96, 413-429.

Schaeffer, J. T., and C. A. Doswell III, 1979: "On the Interpolation of a Vector Field," Mon. Wea. Rev., 107(4), 458-476.

Shukla, J., and K. R. Saha, 1974: "Computation of Non-divergent Streamfunction and Irrotational Velocity Potential from the Observed Winds," Mon. Wea. Rev., 102(6), 419-425.

1. REPORT NO.	2. GOVERNMENT ACCESSION NO.	3. RECIPIENT'S CATALOG NO.
NASA CR-3378		

4. TITLE AND SUBTITLE	5. REPORT DATE
Case Studies of Clear Air Turbulence Using the Diagnostic Richardson Number Tendency Formulation	January 1981
	6. PERFORMING ORGANIZATION CODE

7. AUTHOR(S)	8. PERFORMING ORGANIZATION REPORT #
John L. Keller and Patrick A. Haines	UDR TR 80-97

9. PERFORMING ORGANIZATION NAME AND ADDRESS	10. WORK UNIT NO.
University of Dayton Research Institute Dayton, Ohio 45469	M-324
	11. CONTRACT OR GRANT NO.
	NAS8-32111

12. SPONSORING AGENCY NAME AND ADDRESS	13. TYPE OF REPORT & PERIOD COVERED
National Aeronautics and Space Administration Washington, D.C. 20546	Contractor Report
	14. SPONSORING AGENCY CODE

15. SUPPLEMENTARY NOTES

Marshall Technical Monitor: Dennis W. Camp
Final Report

16. ABSTRACT

The results of four case studies of Clear Air Turbulence (CAT) using the Diagnostic Richardson Number Tendency (DRT) formulation are highlighted. The performance of this technique in resolving regions of documented CAT encounters is encouraging. Its operational adaptability appears particularly attractive in that input data can be supplied by the currently operational Rawinsonde system.

Two CAT indices are calculated deterministically, sensing synoptic-scale changes in static stability and vertical wind shear conducive for supporting mesoscale CAT layers. These two indices reveal volumes of the troposphere which act as "source regions" for patches of CAT. The first, the time to reach the critical Richardson number necessary for the initiation of turbulent conditions, was first used by Oard (1974). A second index is devised which is an adaptation of Roach's (1970) work relating synoptic-scale and mesoscale energetical coupling and gives more information on the relative intensity of these "source regions." The output from the DRT computer module highlights specific regions of the atmosphere which can be interpreted operationally in terms of a CAT encounter probability.

17. KEY WORDS	18. DISTRIBUTION STATEMENT
Clear Air Turbulence	Unclassified - Unlimited Subject Category 47

19. SECURITY CLASSIF. (of this report)	20. SECURITY CLASSIF. (of this page)	21. NO. OF PAGES	22. PRICE
Unclassified	Unclassified	56	A04

For sale by National Technical Information Service, Springfield, Virginia 22161

NASA-Langley, 1981